Biosystems, Foster City, CA, USA) was used for PCR amplification. The amplification program used was 35 cycles of 30 s at 94°C, 30 s at 64°C, and 40 s at 72°C, with a final incubation of 7 min at 72°C.

Flow cytometry and cell sorting

Cultured cells were incubated with enzyme-free Hank's-based Cell Dissociation Buffer (Invitrogen) for 30 min at 37°C and gently dissociated into single cells. The cells were then washed with PBS twice, probed with biotinylated-SM/C-2.6 (23) antibody for 15 min at room temperature, and stained with phycoerythrin-conjugated strepavidin (12-4312; eBioscience, San Diego, CA, USA) for 15 min at room temperature. Dead cells were excluded from the plots based on propidium iodide staining (Sigma), and SM/C-2.6-positive cells were collected using a FACS Vantage instrument (Becton Dickinson, San Jose, CA, USA). Sorted cells were plated (1×10^4 cells/well) with differentiation medium in 96-well plates (Falcon) coated with Matrigel (008504; BD Bioscience). The medium was changed every 5 d, and 7 d after plating the cultured cells were analyzed.

Intramuscular cell transplantation (primary transplantation)

Recipient mice were injected with 50 μl of 10 μM cardiotoxin (CTX; Latoxan, Valence, France) (30) in the LTA muscle 24 h before transplantation (31). CTX is a myotoxin that destroys myofibers, but not satellite cells, and leaves the basal lamina and microcirculation intact. Since proliferation of host myogenic cells may prevent the incorporation of transplanted cells, recipient mdx mice (15) received 8 cGy of systemic irradiation (32) 12 h before transplantation to block muscle repair by endogenous cells. An average of 4.53×10^4 ES-derived SM/C-2.6-positive or -negative cells were washed twice with 500 μl of PBS, resuspended in 20 μl of DMEM, and injected into the LTA muscle of recipient mdx mice using an allergy syringe (Becton Dickinson). Mdx mice, which are derived from the CL/B16 strain, were used as the recipient mice in all experiments. Similarly, D3 ES cells, which are derived from the 129X1/SvJ ES cells, were used in all experiments. The major histocompatibility complex (MHC) of mdx mouse and D3 cells are very similar, both possessing type *b* MHC H2 haplotypes. All animal-handling procedures followed the Guild for the Care and Use of Laboratory Animals published by the U.S. National Institutes of Health (NIH Publication No. 85-23, revised 1996) and the Guidelines of the Animal Research Committee of the Graduate School of Medicine, Kyoto University.

Secondary transplantation

The LTA muscles of recipient mice were collected 8 wk after the primary transplantation. The muscles were minced and digested into single cells with 0.5% collagenase type I (lot S4D7301; Worthington Biochemical Corp., Lakewood, NJ, USA). After washing with PBS and filtration through a 100 μm filter, Pax7-positive cells were sorted by FACS using the SM/C-2.6 antibody. SM/C-2.6-positive cells (200 cells/mouse) were injected into preinjured LTA muscles of secondary recipient mice. The LTA muscles were analyzed 8 wk after transplantation.

Isolation and immunostaining of single fibers

To detect muscle satellite cells attaching to single fibers with Pax7, muscle fibers from the LTA muscle of recipient mice were prepared essentially according to the method of Bischoff in Rosenblatt *et al.* (33). Briefly, dissected muscles were incubated in DMEM containing 0.5% type I collagenase (Worthington) at 37°C for 90 min. The tissue was then transferred to prewarmed DMEM containing 10% FBS. The tissue was gently dissociated into single fibers by trituration with a fire-polished wide-mouth Pasteur pipette. Fibers were transferred to a Matrigel-coated 60 mm culture dish (Falcon) and fixed in 4% PFA for 5 min at room temperature. Fibers were permeabilized with 0.1% Triton X-100 in PBS for 10 min, and nonspecific binding was blocked by incubation in 5% skim milk for 10 min at room temperature. Primary mouse monoclonal antibodies against mouse Pax7 were applied for 12 h at 4°C. Antibodies were detected using the secondary antibodies described above.

Statistics

Data are presented as means ± SD. For comparison of the numbers of MHC and Pax7-positive cells in the sorted SM/C-2.6-positive and -negative fractions and the numbers of GFP-positive muscle fascicles and GFP/Pax7-double-positive cells in reinjured and noninjured groups, the unpaired Student's *t* test was used, and a value of $P < 0.05$ was considered to be statistically significant.

RESULTS

Myogenic lineage cells are effectively induced from mES cells *in vitro*

EBs were formed in hanging drop cultures for 3 d followed by an additional 3 d in suspension cultures (**Fig. 1*A***). These EBs were then plated onto Matrigel-coated 48-well plates in differentiation medium, which contained 5% HS. This culture method is a modified version of the classical ES cell differentiation method (25) and the skeletal muscle single fiber culture method (33). After plating, EBs quickly attached to the bottom of the coated dishes, and spindle-shaped fibers appeared surrounding the EBs by the seventh day of plating (d 3+3+7; Fig. 1*B*). As these spindle fibers grew, they began to fuse with each other, forming thick multinucleated fibers resembling skeletal myofibers (Fig. 1*C, D*). At the same time we observed spontaneous contractions by the fibers (Supplemental Videos 1 and 2), a trait commonly seen in cultured skeletal muscle fibers. Immunostaining showed that these fused fibers were positive for skeletal-muscle-specific MHC (Fig. 1*E*). Furthermore, cells expressing muscle regulatory factor (MRF) proteins, including Pax7 (Fig. 1*F*), Myf5 (Fig. 1*G*), MyoD (Fig. 1*H*), and myogenin (Fig. 1*I*) were observed. On d 3 + 3 + 14, the average number of MHC-positive wells was 73.6 ± 5.8% (n=144). In all the MHC-positive wells, cells expressing Pax7, an essential transcription factor in satellite cells, were also observed. Double staining for Pax7 and MyoD confirmed the existence of cells staining for Pax7 alone, indicating the presence of quiescent-state satellite cells (34) within the culture (Supplemental Fig. 1). Next, the time course of MRF expression was examined by RT-PCR (Fig. 1*J*). Expression of Pax3 and Pax7 both peaked on d 3 + 3 +

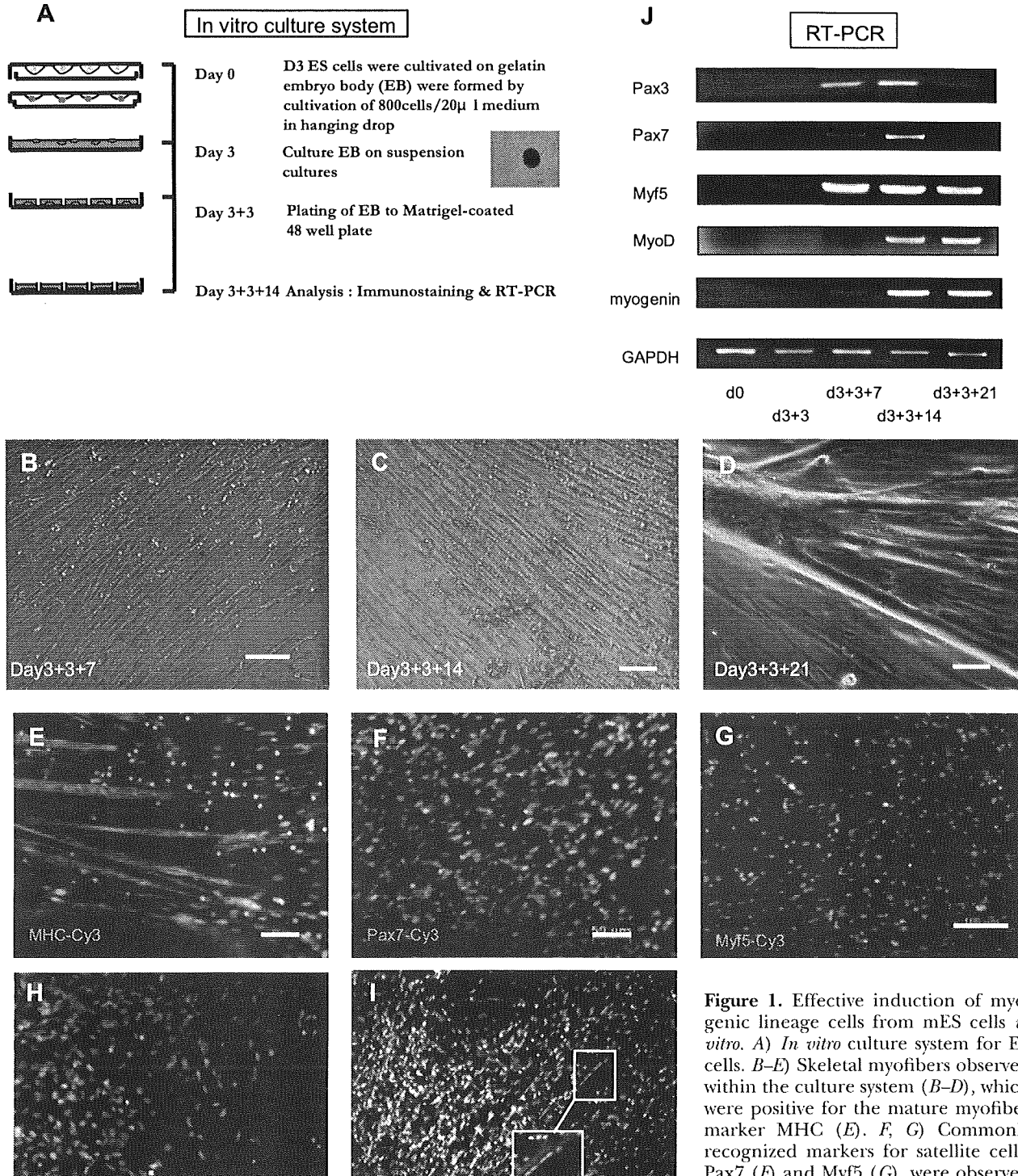

Figure 1. Effective induction of myogenic lineage cells from mES cells *in vitro*. *A*) *In vitro* culture system for ES cells. *B–E*) Skeletal myofibers observed within the culture system (*B–D*), which were positive for the mature myofiber marker MHC (*E*). *F, G*) Commonly recognized markers for satellite cells, Pax7 (*F*) and Myf5 (*G*), were observed in the cultures. *H, I*) MyoD-positive (*H*) and myogenin-positive fibers (*I*) were also observed in the cultures. White boxes indicate multinucleated myotubes (*I*). *J*) RT- PCR expression of MRFs including Pax3, Pax7, Myf5, MyoD, and myogenin in ES cells in our novel culture system at d 0, 3 + 3, 3 + 3 + 7, 3 + 3 + 14, and 3 + 3 + 21. Scale bars = 50 μm (*A–F*); 100 μm (*G–I*).

14, but Myf5, MyoD, and myogenin continued to be expressed after d 3 + 3 + 14.

Thus, using Matrigel plates and differentiation medium containing HS, myogenic lineages including Pax7-positive satellite-like cells were successfully induced from mES cells.

A novel antibody, SM/C-2.6, can enrich for Pax7-positive satellite-like cells derived from ES cells

To examine the characteristics of ES-derived Pax7-positive satellite-like cells, we needed to isolate these cells from the culture. Since Pax7 is a nuclear protein rather than a

surface marker, anti-Pax7 antibodies cannot be used for living cell separation by FACS. Therefore, a novel antibody, SM/C-2.6 (23), was used to detect satellite cells. SM/C-2.6 detects quiescent adult mouse satellite cells, as well as satellite cells in neonatal muscle tissue, as determined by immunostaining (Supplemental Fig. 2). RT-PCR confirmed that sorted SM/C-2.6-positive cells expressed Pax3, Pax7, Myf5, and c-met, whereas sorted SM/C-2.6-negative cells did not (Supplemental Fig. 3). Thus, the SM/C-2.6 antibody was shown to be useful for isolating living satellite cells by FACS.

We collected all the differentiated ES cells (1×10^6 cells) from cultures on d 3 + 3 + 14. FACS analysis using the SM/C-2.6 antibody showed that 15.7% of the cells were SM/C-2.6 positive (**Fig. 2*A***). RT-PCR analysis revealed that sorted SM/C-2.6-positive cells strongly expressed Pax3, Pax7, Myf5, c-met, and M-cadherin (Fig. 2*B*). Using a cytospin preparation of sorted SM/C-2.6-positive cells, we also confirmed the expression of M-cadherin (Fig. 2*C*) and Pax7 (Fig. 2*D;* 70.7±16.5% and 59.9±1.1% positive, respectively); only 2.3 ± 0.49% of the sorted SM/C-2.6-negative cells expressed M-cadherin, and 2.7 ± 0.1% expressed Pax7. Thus, the SM/C-2.6 antibody could enrich for satellite-like cells derived from mES cells *in vitro.*

ES-derived satellite-like cells have strong myogenic potential *in vitro*

To evaluate the myogenic potential of ES-derived SM/C-2.6-positive satellite-like cells *in vitro,* both SM/C-2.6-positive and -negative cells were sorted by FACS and plated in 96-well Matrigel-coated plates (see Fig. 4A). One week after cultivation, the number of muscle fibers in the wells was assessed. Although there were fibroblast-like and endothelium-like cells, MHC-positive fibers (787.3±123.7/well, 10.7±0.8% of the total cells per well, n=3) and Pax7-positive cells (222±81.4/well, 2.9±1.1% of the total cells per well, n=9) were observed in the SM/C-2.6-positive wells. In contrast, very few MHC-positive fibers (8.75±32.6/well, n=15; 0.12±0.46%) or Pax7-positive cells (2.6±2.0/well, n=8; 0.03±0.01%) were seen in the SM/C-2.6-negative wells

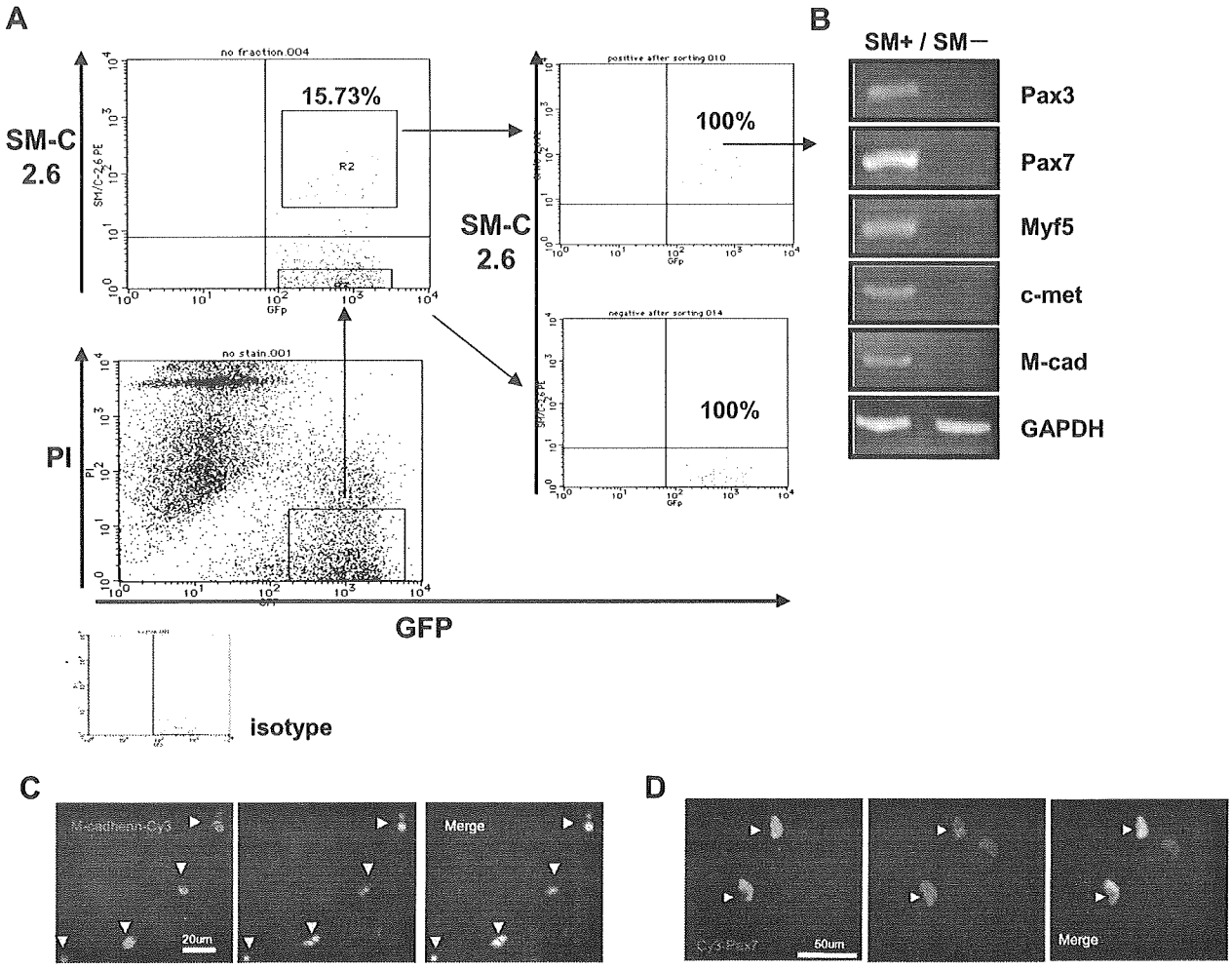

Figure 2. A novel antibody, SM/C-2.6, can enrich Pax7-positive satellite-like cells derived from ES cells. *A*) FACS data of cultured ES cells at d 3 + 3 + 14 indicate that 15.7% of total cultured cells are SM/C-2.6-positive cells. *B*) RT-PCR of the SM/C-2.6-positive fraction showed strong expression of Pax3, Pax7, Myf5, c-met, and M-cadherin. Immunostaining of a cytospin preparation of the sorted SM/C-2.6-positive cells showed that these cells were positive for M-cadherin (*C*), and Pax7 (*D*) (white arrowheads). Scale bars = 20 μm (*C*); 50 μm (*D*).

(both $P<0.05$; **Fig. 3**). Thus, ES-derived satellite-like cells isolated using the SM/C-2.6 antibody possess strong myogenic potential *in vitro*.

Damaged muscle can be repaired by transplantation of ES-derived satellite-like cells

To examine the myogenic potential of ES-derived satellite-like cells *in vivo*, SM/C-2.6-positive and -negative cells were transplanted into conditioned mdx mice (15). The LTA muscles of recipient mdx mice were preinjured with CTX (primary injury; ref. 30) 24 h prior to transplantation, and mice were exposed to 8 cGy of γ-irradiation (whole body) 12 h prior to transplantation (**Fig. 4A**). GFP-positive ES cells were used as donor cells in this experiment. GFP$^+$ES-derived SM/C-2.6-positive and -negative cells were directly injected into the predamaged LTA muscles. The recipient mice were analyzed 3 wk post-transplantation. By fluorescence stereomicroscopy, GFP-positive tissues were clearly observed within the LTA muscles injected with SM/C-2.6-positive cells (Fig. 4*B* and **Table 1**). In contrast, no GFP-positive tissue was observed in muscles injected with SM/C-2.6-negative cells (Fig. 4*C*). These GFP-positive tissues were further confirmed by diaminobenzidine staining using anti-GFP and a peroxidase-conjugated secondary antibody (Supplemental Fig. 4) to exclude the possibility of autofluorescence of the muscle tissues. Immunostaining with anti-MHC confirmed that these GFP-positive tissues were mature skeletal myofibers (Fig. 4*D*). In addition, GFP/Pax7 double-positive cells were observed within the LTA muscles of the recipient mice (Fig. 4*E* and Supplemental Fig. 5) and in isolated single fibers (Fig. 4*F* and Table 1). The GFP-positive cells were also confirmed to be positive for other satellite cell markers such as Myf5 and M-cadherin (Supplemental Figs. 6 and 7). These GFP/Pax7-double-positive cells were located along the periphery of the muscle fascicle. With laminin immunostaining we verified that the location of the GFP-positive mononuclear cells was between the basal lamina and the muscle cell plasma membrane, a location consistent with the anatomical definition of satellite cells

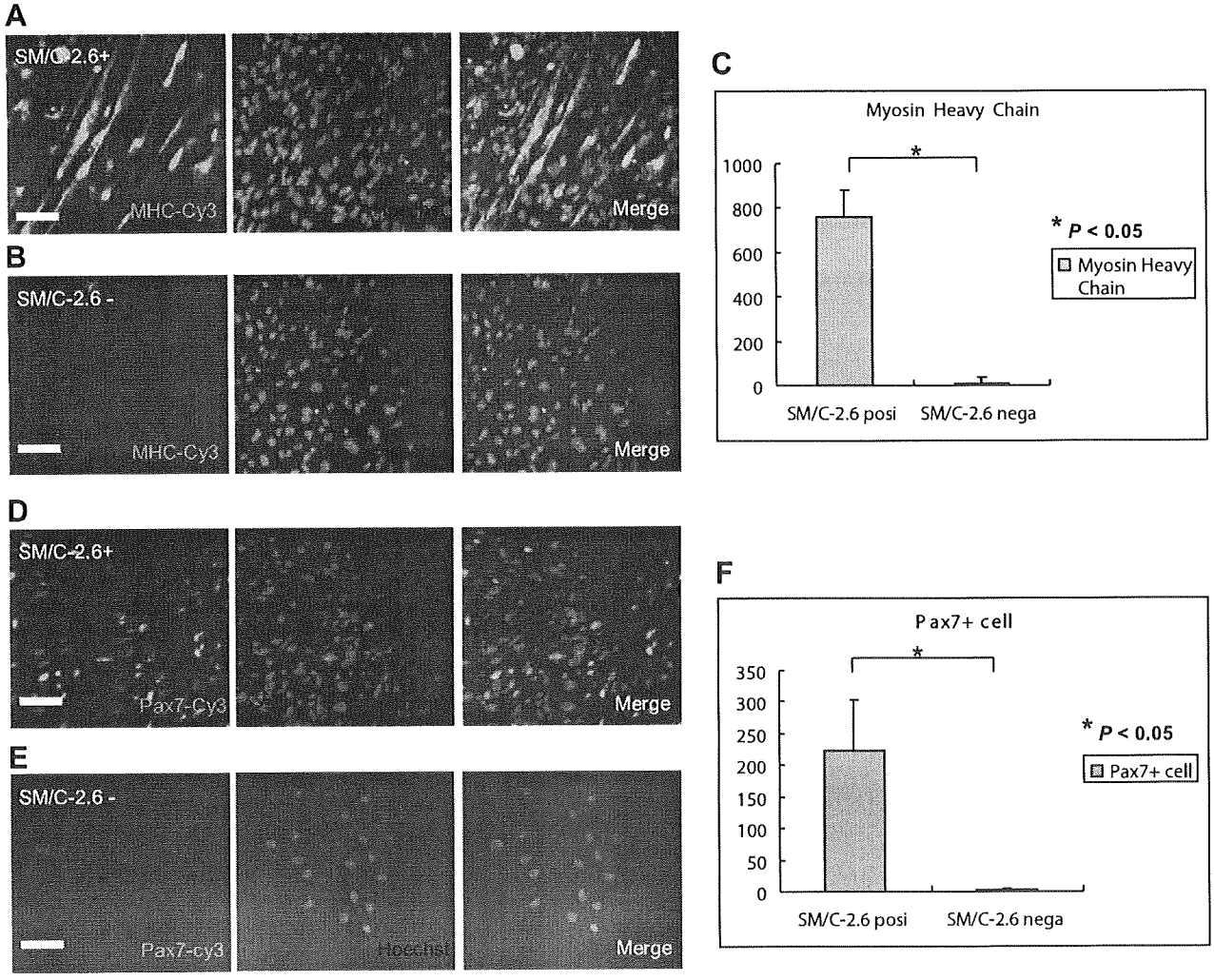

Figure 3. ES-derived satellite-like cells have strong myogenic potential *in vitro*. Immunostaining detected an abundant number of MHC-positive fibers and Pax7-positive cells in SM/C-2.6-positive cell culture (*A, D*) but not SM/C-2.6-negative cells (*B, E*) after 1 wk in culture. Scale bars = 50 μm. Significant differences were observed in the number of MHC-positive fibers and Pax7-positive cells per well between sorted SM/C-2.6-positive and -negative cell cultures (*C, F*).

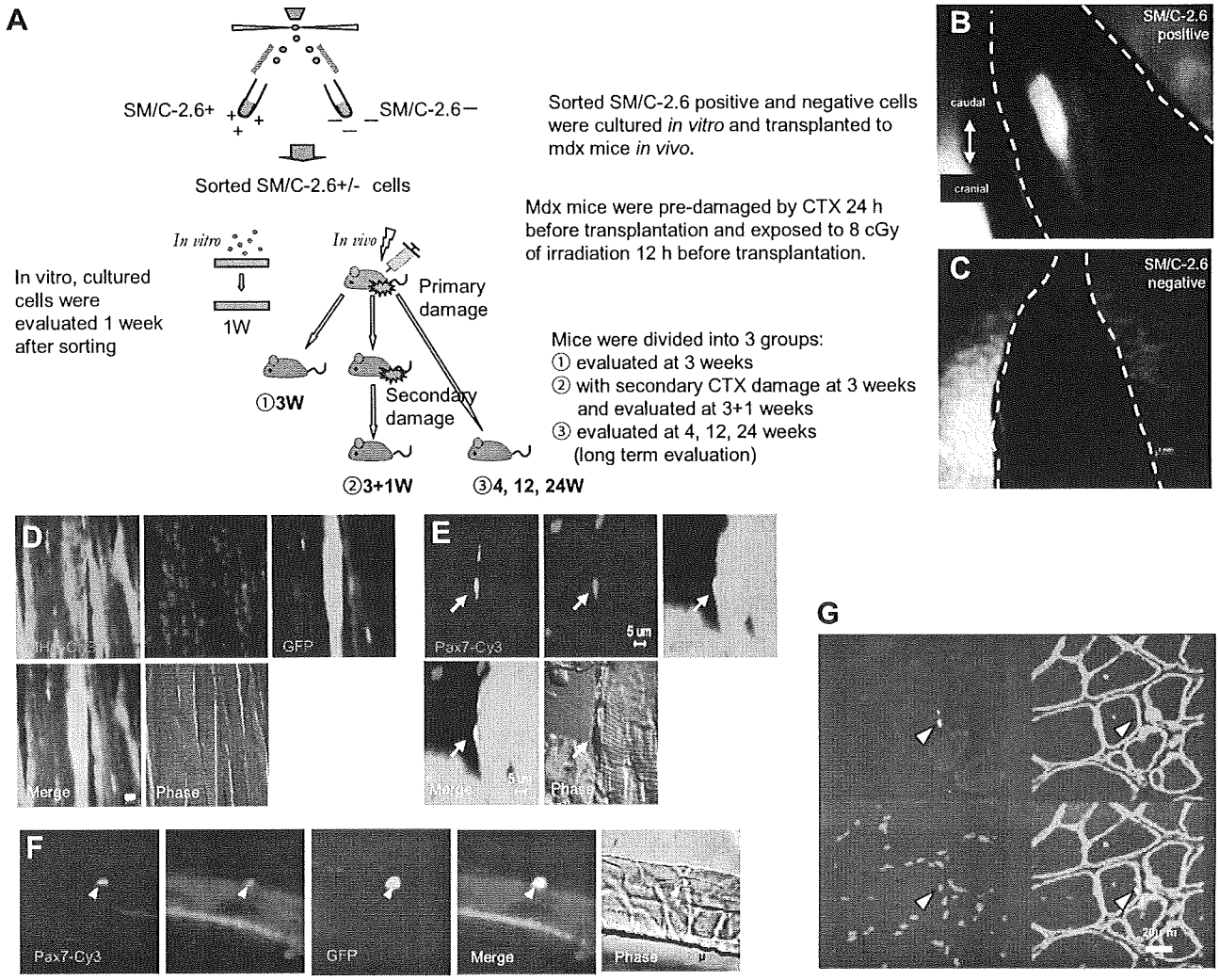

Figure 4. ES-derived satellite-like cells can repair damaged muscle *in vivo*. *A*) Methods for *in vitro* and *in vivo* analysis of sorted SM/C-2.6-positive and -negative cells derived from mES cells. *B, C*) ES-derived GFP-positive tissue engrafted to the LTA muscle of a recipient mouse that received SM/C-2.6-positive cells (*B*) but SM/C-2.6-negative cells (*C*). *D*) Grafted GFP-positive tissues were histologically MHC positive. *E*) GFP/Pax7-double-positive cells were observed in mice that received SM/C-2.6-positive cells by anti-Pax7 immunostaining. *F*) GFP/Pax7-double-positive cells were also confirmed by immunostaining of isolated single fibers. *G*) Laminin immunostaining indicated that the GFP-positive cells were located between the basal lamina and the muscle cell plasma membrane, which is consistent with the anatomical definition of muscle satellite cells. Scale bars = 1 mm (*B, C*); 15 μm (*D*); 5 μm (*E*); 20 μm (*F, G*).

(Fig. 4*G*). In contrast, in mice transplanted with SM/C-2.6-negative cells, GFP-positive tissues were rarely observed, and none of the GFP-positive cells were positive for skeletal MHC. H&E staining indicated that these GFP-positive tissues were surrounded by inflammatory cells (Supplemental Fig. 8), suggesting that these nonmyogenic tissues may undergo phagocytosis. These results demonstrate that ES-derived SM/C-2.6-positive satellite-like cells could be engrafted *in vivo* and repair damaged muscle tissues of the host.

Engrafted ES-derived satellite-like cells function as satellite cells following muscle damage

Muscle satellite cells are generally considered to be self-renewing monopotent stem cells that differentiate into myoblasts and myofibers to repair damaged skeletal muscles. To determine whether these engrafted GFP^+ES-derived satellite-like cells are functional stem cells, we injured the LTA muscle of primary recipient mice 3 wk after primary transplantation with GFP^+SM/C-2.6-positive cells. This experiment let us assess the ability of satellite-like cells to repair damaged muscle fibers and self-renew *in vivo* (14). The LTA muscles were removed and analyzed 1 wk after the secondary injury (reinjured group). Mice that were initially injected with GFP^+SM/C-2.6-positive cells without a second injury were used as a control (nonreinjured group). These control mice were analyzed 3 or 4 wk after transplantation (Fig. 4*A*). GFP-positive muscle fascicles were counted in sections of both reinjured and nonreinjured muscle (**Fig. 5*A, B***). In the reinjured group 461.7 ± 117.4 (n=6; per view, ×100) GFP-positive muscle fascicles were observed. In comparison, only 136.7 ± 27.9 (n=4) and 168.7 ± 72.9 (n=6; per view, ×100) GFP-positive muscle fascicles were evident in

TABLE 1. *Transplantation of reinjured and nonreinjured mice and long-term evaluation*

Group	TA with GFP$^+$ fascicles [n(%)][a]	Mouse	Cells/TA injected (n)	GFP$^+$ fascicles/TA (avg)[b]	GFP$^+$/Pax7$^+$ cells/TA (avg)[c]	Engraftment efficiency
SM/C-2.6$^+$						
3W	4/8 (50%)	1	1.75×10^4	125.3	5.3	
		2	3.5×10^4	111.1	7.1	
		3	5×10^4	134.2	5.1	
		4	8×10^4	176.1	4.2	
Mean			$4.5 \pm 2.6 \times 10^4$	136.7 ± 27.0	5.4 ± 1.2	0.30%
4W	6/9 (66.67%)	1	2×10^4	77.3	6.1	
		2	1.3×10^5	153.2	4.6	
		3	5×10^4	163.1	6.8	
		4	3.5×10^4	168.9	5.1	
		5	8×10^4	281.1	7.2	
		6	1.75×10^4	169.4	6.2	
Mean			$3.6 \pm 2.5 \times 10^4$	168.7 ± 72.9	6 ± 1	0.47%
3 + 1W	6/8 (75%)	1	2×10^4	581.2	11.2	
		2	1.3×10^5	370.3	11.5	
		3	5×10^4	586.6	10.1	
		4	3.5×10^4	486.6	5.9	
		5	8×10^4	347.1	15.3	
		6	1.75×10^4	542.9	10.8	
Mean			$5.5 \pm 4.3 \times 10^4$	461.7 ± 117.3	10.8 ± 3	0.84%
12W	3/5 (60%)	1	2×10^4	391.5	9.7	
		2	5×10^4	266	9.3	
		3	8×10^4	280.2	6	
Mean			$5 \pm 3 \times 10^4$	312.6 ± 68.7	8.3 ± 2	0.59%
24W	1/2 (50%)	1	2×10^4	58.62	3.45	
Mean			2×10^4	58.62	3.45	0.20%
SM/C-2.6$^-$						
3W	0/8 (0%)	1–8	$1–8 \times 10^4$	0	0	0%
4W	0/9 (0%)	1–9	$1.3–8 \times 10^4$	0	0	0%
3 + 1W	0/8 (0%)	1–8	$1.75–13 \times 10^4$	0	0	0%
12W	0/5 (0%)	1–8	$2–8 \times 10^4$	0	0	0%
24W	0/2 (0%)	1–2	2×10^4	0	0	0%

Serial transplantation

	Primary transplantation		Secondary transplantation		
Mouse	Cells injected	Collected GFP$^-$ cells/TA	Cells injected	GFP$^+$ fascicles/TA	Engraftment efficiency
1	2×10^4	3253	200	29.3	14.7%
2	2×10^4	2277	200	28.6	14.3%
Mean	2×10^4	2765	200	29 ± 0.5	14.5%

TA, tibialis anterior; 3W, nonreinjured group analyzed 3 wk after cell transplantation; 4W, nonreinjured group analyzed 4 wk after cell transplantation; 3 + 1W, reinjured group reinjured 3 wk after cell transplantation and analyzed 1 wk after reinjury; 12W, long-term engraftment evaluation analyzed 12 wk after cell transplantation; 24W, long-term engraftment evaluation analyzed 24 wk after cell transplantation. [a]Percentage of TA that had engrafted with GFP$^+$ fibers was calculated as number of TAs with GFP$^+$ fibers/total TAs injected with cells. [b]Average determined from number of GFP$^+$ muscle fascicles counted per field at ×100 in 10 fields. [c]Average determined from number of GFP$^+$/Pax7+ cells counted per field at ×100 in 10 fields.

the nonreinjured groups at 3 and 4 wk, respectively, after transplantation (Fig. 5*B* and Table 1). Furthermore, we also observed that many GFP-positive muscle fibers had a typical central nucleus in the reinjured group (Fig. 5*C*), indicating regenerating muscle fibers. Taken together, these results suggest that these GFP-positive muscle tubes were freshly regenerated by the engrafted GFP$^+$ ES-derived satellite-like cells in response to the second injury. Surprisingly, immunostaining with anti-Pax7 revealed an increase in number of GFP/Pax7-double-positive cells in the reinjured group (10.8±3.0/view compared to 5.4±1.2, and 6.0±1.0 in the nonreinjured group; Fig. 5*D* and Table 1). This result strongly suggests that engrafted ES-derived satellite-like cells not only self-renewed but also expanded in number, possibly replacing the recipient satellite cells lost because of excessive repair of skeletal muscle in response to the second injury.

ES-derived satellite-like cells are capable of long-term engraftment in recipient muscles

Long-term engraftment is an important characteristic of self-renewing stem cells. If these ES-derived satellite-

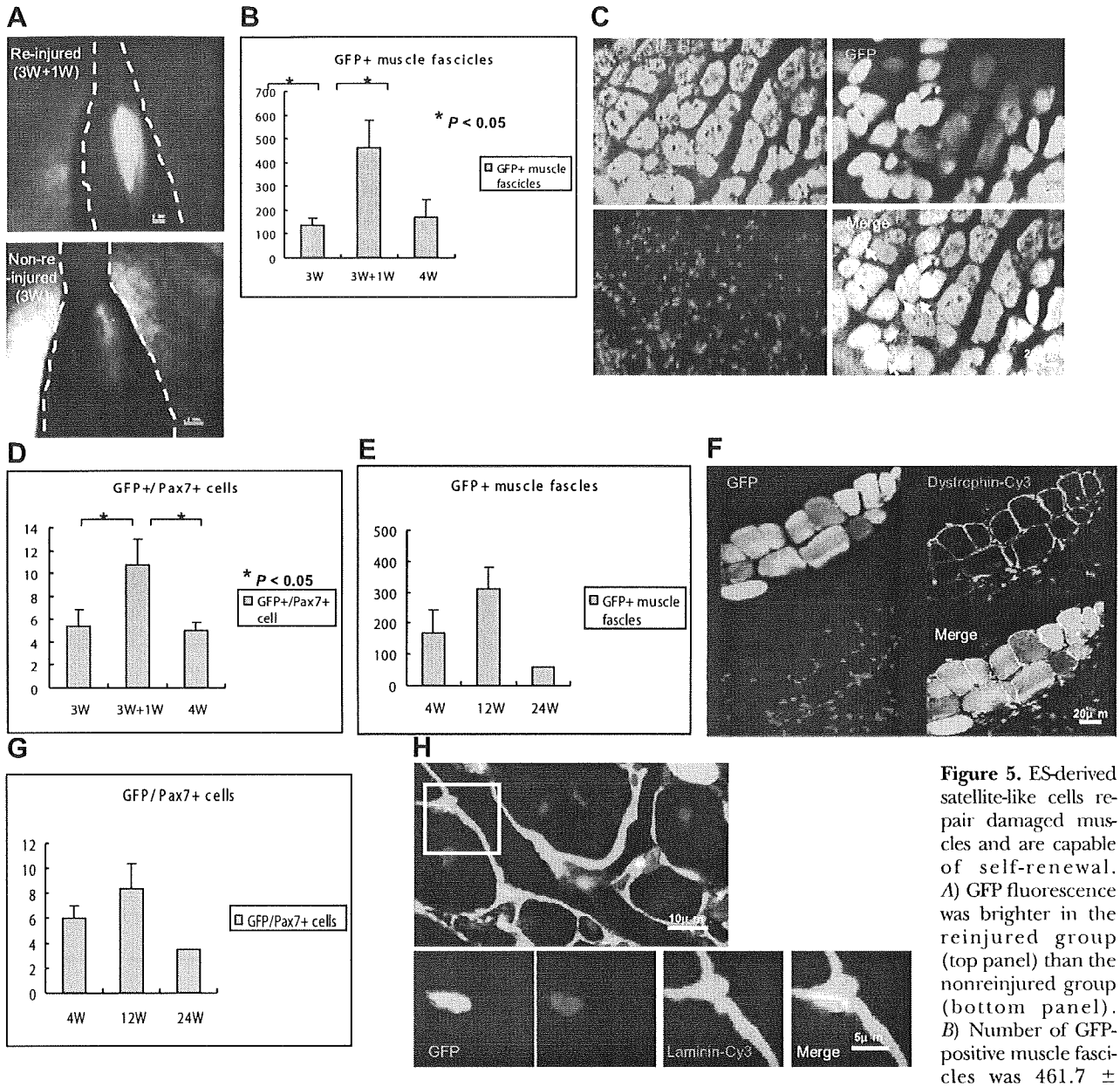

Figure 5. ES-derived satellite-like cells repair damaged muscles and are capable of self-renewal. *A*) GFP fluorescence was brighter in the reinjured group (top panel) than the nonreinjured group (bottom panel). *B*) Number of GFP-positive muscle fascicles was 461.7 ± 117.3 in the reinjured group (3W+1W) and 136.7 ± 27.9 and 168.7 ± 72.9 in the nonreinjured group at 3 wk (3W) and 4 wk (4W), respectively. *C*) GFP-positive fibers were confirmed to be MHC positive and contained central nuclei (arrows). *D*) Number of GFP/Pax7-double-positive cells also increased significantly in the reinjured group (10.8±3.0 cells at 3W+1W) compared to the nonreinjured group (5.4±1.2 and 6.0±1.0 at 3W and 4W, respectively). *E*) In long-term evaluations, number of GFP-positive muscle fascicles at 12 wk (12W) increased relative to number at 4 wk after transplantation [312.6±68.7 (n=3) *vs.* 168.7±72.9]. However, a decrease was observed at 24 wk (58.6; n=1). *F*) Immunostaining showed dystrophin (red) surrounding the donor-derived GFP-positive fibers (green), 24 wk after transplantation of SM/C-2.6-positive cells. *G*) Results similar to *E* were observed with the number of GFP/Pax7-double-positive cells. *H*) A GFP-positive cell beneath the basal lamina was observed. Scale bars = 1 mm (*A*); 20 μm (*C*); 20 μm (*F*); 10 μm (*H*, top panel); 5 μm (*H*, bottom panels).

like cells function as normal stem cells in skeletal muscle, they should be able to reside within the tissue for long periods of time and undergo asymmetric cell divisions to maintain the number of satellite cells and to generate muscle fibers. To examine this stem cell function, we analyzed the recipient mice at 4, 12, and 24 wk after transplantation. Intriguingly, in the LTA muscle of mdx mice transplanted with SM/C-2.6-positive cells, the number of GFP-positive fascicles at 12 wk increased over that at 4 wk [12.6±68.7 (n=3) *vs.* 168.7±72.9; Fig. 5*E*] but decreased by 24 wk (58.6; n=1). These engrafted GFP-positive tissues were confirmed to be MHC positive through immunostaining (Supplemental Fig. 9), and surrounding these GFP-positive fibers, dystrophin was observed (Fig. 5*F*). The numbers of GFP/Pax7-double-positive cells were maintained from week 4 to week 24 (Fig. 5*G*, Table 1, and Supplemental Fig. 10) and the location of GFP-positive cells under the basal lamina meets the anatomical definition of satellite cells (Fig. 5*H*). No teratomas were

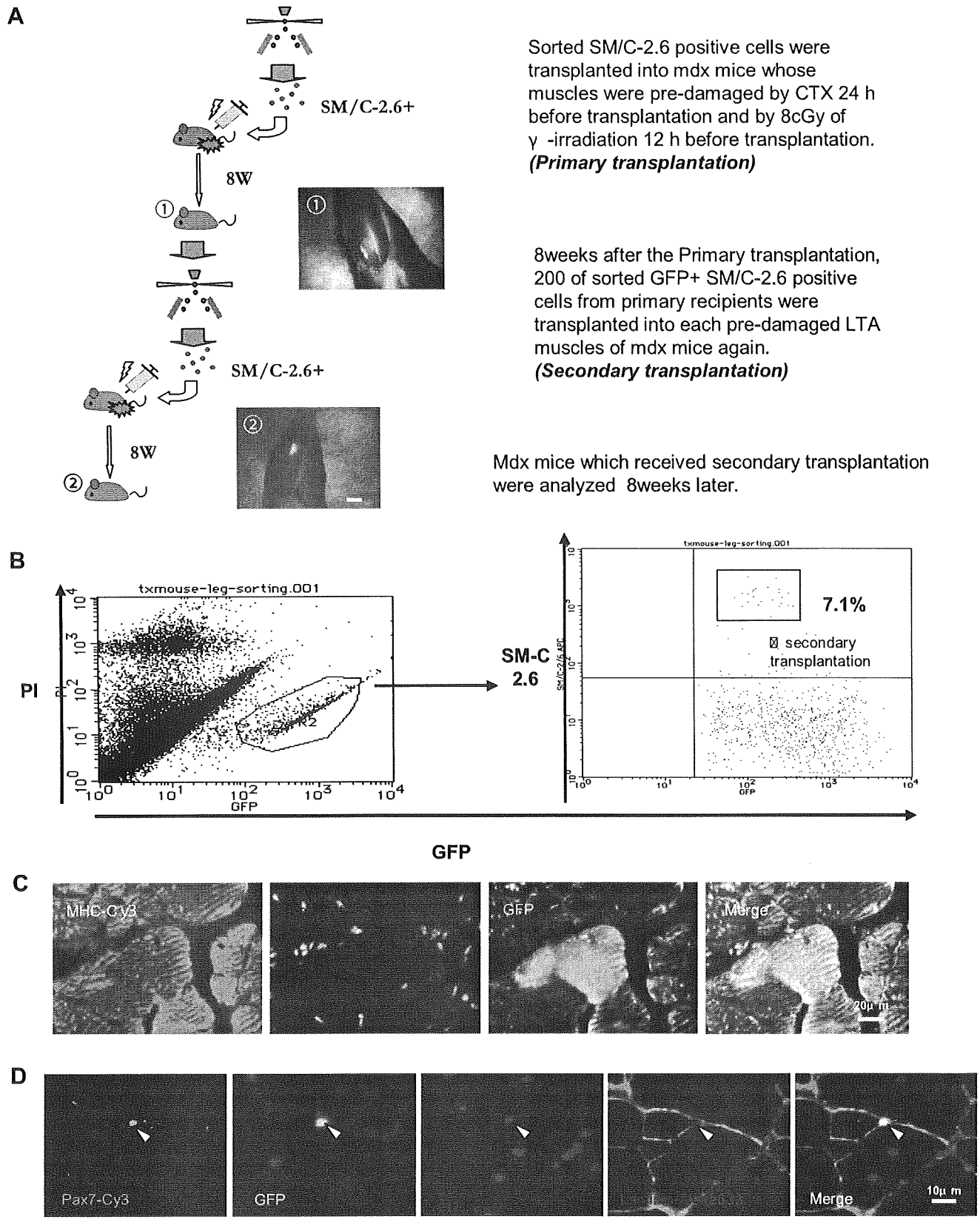

Figure 6. ES-derived satellite-like cells can be secondarily transplanted. *A*) SM/C-2.6-positive cells (2.5×10^4) were transplanted into the LTA muscle of recipient mice in primary transplantation, and as few as 200 SM/C-2.6-positive cells collected from the primary recipients were retransplanted (secondary transplantation) into the LTA muscle of secondary recipient mice. *B*) FACS data of primary transplantation indicated that 7.1% of engrafted (GFP-positive) cells were SM/C-2.6-positive. *C*) Eight weeks after secondary transplantation, immunostaining of LTA muscle for MHC showed that engrafted ES-derived GFP-positive tissues formed mature skeletal muscle fibers. *D*) GFP/Pax7-double-positive cells (arrowhead) located beneath the basal lamina were observed within GFP-positive LTA muscle of secondary recipient mice. Scale bars = 2 mm (*A*); 20 μm (*C*); 10 μm (*D*).

found in recipient mice transplanted with SM/C-2.6-positive cells. Thus, ES-derived satellite-like cells effectively engrafted and provided long-term stem cells, which played an important role in maintenance of the integrity of the surrounding muscle tissue.

ES-derived satellite-like cells can be secondarily transplanted

For a more thorough characterization of the ES-derived satellite-like cells, we performed serial transplantations. Eight weeks after the primary cell transplantation with 2×10^4 SM/C-2.6-positive cells, the LTA muscles of the primary recipient mice were dissected to isolate the engrafted ES-derived cells, 2765 ± 685.9 (n=2; **Fig. 6*A***). The GFP^+/SM/C-2.6-positive cells within the engrafted cells were sorted by FACS (204±33.9; n=2), and only 200 GFP+/SM/C-2.6-positive cells/mouse were transplanted into predamaged LTA muscles of mdx mice (Fig. 6*B*). Eight weeks later (16 wk after the primary transplantation), the recipient mice were analyzed. GFP-positive tissue in the LTA muscle of the secondary recipient mice was observed (Fig. 6*A*). The GFP-positive tissues were confirmed to be MHC-positive mature skeletal muscle (Fig. 6*C*), and surrounding these engrafted GFP-positive skeletal muscle fascicles, dystrophin was observed (Supplemental Fig. 11). GFP/Pax7-double-positive cells located beneath the basal lamina were also detected in the engrafted tissue (Fig. 6*D*). Thus, with only 200 GFP^+SMC/2.6-positive cells, injured skeletal muscle and Pax7+ cells were successfully restored in the secondary recipients. These findings demonstrate that stem cell fraction contained within SM/C-2.6-positive cells was enriched *in vivo* through transplantation.

DISCUSSION

Many attempts have been made to induce mES cells into the skeletal muscle lineage, with hanging drop cultures for EB formation being the most widely applied method (25). However, although EBs contain cells derived from all 3 germ layers, effective induction of mES cells into the myogenic lineage, including myogenic stem cells (satellite cells), has not yet been achieved. Because of the lack of adequate surface markers, purifying ES-derived myogenic precursor/stem cells from differentiated mES cells *in vitro* has been difficult. To overcome these problems, we modified the classic EB culture system by combining it with aspects of the single-fiber culture method. Single-fiber culture (33) has been used for functional evaluation of satellite cells. When a single myofiber is plated on a Matrigel-coated plate with DMEM containing HS, satellite cells migrate out of the fiber and differentiate into myoblasts to form myofibers *in vitro*. Matrigel allows the migrating satellite cells to proliferate before differentiating and fusing into large multinucleated myotubes (35). We hypothesized that this Matrigel environment might be suitable for ES cell differentiation into satellite cells and myoblasts. Therefore, we introduced Matrigel and HS into the classic EB culture system and established an efficient induction system for myogenic lineage cells, including cells expressing Pax7, a commonly recognized marker for skeletal muscle stem cells. Furthermore, we also successfully enriched ES-derived Pax7-positive myogenic precursor/stem cells using the SM/C-2.6 antibody.

The steps in ES cell induction are thought to be homologous to normal embryogenesis. During normal skeletal myogenesis, the initial wave of myogenic precursor cells in the dermomyotome express Myf5/MRF4 and Pax3, followed by a wave of Pax3/Pax7 expression (36). These waves of myogenesis act upstream of the primary myogenic transcription factor MyoD (37-39). In myotome formation skeletal myogenesis begins with myoblasts, termed somitic myoblasts, which appear at approximately E8.5, followed by the appearance of embryonic myoblasts (E11.5), fetal myoblasts (E16.5), and, ultimately, satellite cells, which are responsible for postnatal muscle regeneration (40). Our RT-PCR results (Fig. 1*J*) showed an earlier appearance of Pax3 expression, on d 3 + 3, followed by Pax3/Pax7 expression on d 3 + 3 + 7 and stronger expression of Pax3 than Pax7. These results resemble normal myogenesis, in which the primary wave of myogenesis is followed by a secondary wave of Pax3/Pax7-dependent myogenesis (41). Considering that in the time course of myogenesis satellite cells emerge during late fetal development, ES-derived Pax7-positive cells were collected on d 3 + 3 + 14 in an attempt to acquire cells that correspond to those of the late fetal to neonatal period. However, RT-PCR results of myogenic factors in SM/C-2.6-positive cells (Fig. 2*B*) indicated that these ES-derived SM/C-2.6-positive cells are a heterogeneous population, because they express not only Pax3 and Pax7 but also Myf5 and c-met. Although further confirmation is needed, we hypothesize that both embryonic/fetal myoblasts expressing Myf-5 and/or c-met and satellite/long-term stem cells expressing Pax3/Pax7 are present.

To confirm that the ES-derived SM/C-2.6-positive cell population contained functional satellite cells, the muscle regeneration and self-renewal capacities were examined. Recently Collins *et al.* established an excellent system in which sequential damage to the muscle of a recipient mouse was applied, to evaluate both muscle regeneration and self-renewal (14) Using their experimental approach, a significant increase in numbers of both ES-derived GFP-positive muscle fascicles and GFP/Pax7-double-positive cells was observed in mice that received a second injury. This result not only demonstrates the myogenic ability of ES-derived cells but also strongly supports the idea that these cells undergo self-renewal *in vivo*.

Analysis of long-term engraftment is an important method to verify self-renewal ability, for 2 reasons. First, ES-derived satellite cells must be able to engraft for long periods of time in order to provide the amount of progeny needed for repairing damaged tissue for an

extended period. In our study the ES-derived GFP-positive skeletal muscle tissues and Pax7-positive cells engrafted up to 24 wk and were located beneath the basal lamina, which is consistent with the anatomical definition of satellite cells. Although the number of GFP-positive fascicles at 24 wk decreased compared to 12 wk, this diminution may be due to the heterogeneity of ES-derived SM/C-2.6-positive cells as we mentioned. Because myoblasts cannot support myogenesis in the long term, we believe that GFP-positive fascicles at 24 wk are products of ES-derived satellite-like cells. Second, one of the potential risks of ES cell transplantation is teratoma formation. Considering clinical applications, it is extremely important to prevent formation of teratomas in the recipients. In our study more than 60 transplanted mice were evaluated through gross morphological and histological examination. There were no teratomas formed in mice that received SM/C-2.6-positive cells, and only 1 teratoma was found among the mice that received SM/C-2.6-negative cells. This result suggests that the risk of tumor formation by the ES cells was eliminated by using sorted SM/C-2.6-positive cells.

In addition to the sequential damage model and the long-term engraftment evaluation, we performed serial transplantations to further confirm the stem cell properties of these ES-derived SM/C-2.6-positive cells. Serial transplantation enables the identification and separation of long-term stem cells from short-term progenitors (42). To eliminate myoblast involvement, we designed a serial transplantation protocol of 8 + 8 wk (*i.e.*, a second transplantation 8 wk after the primary transplantation and an analysis of recipient mice 8 wk after the second transplantation). Strikingly these recollected ES-derived SM/C-2.6-positive cells showed significantly higher engraftment efficiency compared to the primary transplantation. In the previous reports engraftment efficiencies of myoblasts transplantation was ~0.1-0.2%, with the highest reported value being 2% (43-45). This engraftment efficiency is similar to our primary transplantation (0.2-0.8%) as well as the plating efficiency of SM/C-2.6-positive cells *in vitro* (0.07%). In our study as few as 200 recollected ES-derived SM/C-2.6-positive cells were transplanted in the second transplantation, and 29.0 ± 0.47 (n=2) fascicles were observed, which indicates 14.7% of higher engraftment efficiency. Thus, through the serial transplantation, ES-derived stem cell fraction was purified. A comparison of these SM/C-2.6-positive cells before and after injection might help to characterize the stem cell fraction derived from ES cells.

There have been few reports describing transplantation of ES-derived myogenic cells into injured muscles, and the report of engraftable skeletal myoblasts derived from human ES cells represents significant progress (26). Recently Darabi *et al.* (46) have reported that by introducing Pax3 into mouse embryoid bodies, autonomous myogenesis was initiated *in vitro*, and Pax3-induced cells regenerated skeletal muscles *in vivo* by sorting the PDGF-a+Flk-1- cells. The Pax3 expression was not observed until 7 d of differentiation culture, but introduced Pax3 expression pushed EBs to myogenic differentiation. Interestingly, we observed Pax3 expression at d 3 + 3 weakly and d 3 + 3 + 7 strongly, and gene expression process in our culture is very similar to theirs. In prolonged culture using Matrigel and HS, EBs were able to initiate myogenesis without gene modification in our system.

In conclusion, we successfully generated transplantable myogenic cells, including satellite-like cells, from mES cells. The ES-derived myogenic precursor/stem cells could be enriched using a novel antibody, SM/C-2.6. These ES-derived SM/C-2.6-positive cells possess a high myogenic potential, participate in muscle regeneration, and are located beneath the basal lamina where satellite cells normally reside. The self-renewal of these ES-derived satellite-like cells enabled them to survive long-term engraftment, up to 24 wk. Through serial transplantation, these ES-derived SM/C-2.6-positive cells were further enriched and produced a high engraftment efficiency of 14.7%.

Our success in inducing mES cells to form functional muscle stem cells, the satellite-like cells, will provide an important foundation for clinical applications in the treatment of DMD patients. FJ

This work was supported by a Grant-in-Aid for Scientific Research (S) (19109006) and a Grant-in-Aid for Scientific Research (B) (18390298) from the Ministry of Education, Science, Technology, Sports, and Culture of Japan.

REFERENCES

1. Nawrotzki, R., Blake, D. J., and Davies, K. E. (1996) The genetic basis of neuromuscular disorders. *Trends Genet.* **12,** 294–298
2. Emery, A. E. (2002) The muscular dystrophies. *Lancet* **359,** 687–695
3. Michalak, M., and Opas, M. (1997) Functions of dystrophin and dystrophin associated proteins. *Curr. Opin. Neurol.* **10,** 436–442
4. Suzuki, A., Yoshida, M., Hayashi, K., Mizuno, Y., Hagiwara, Y., and Ozawa, E. (1994) Molecular organization at the glycoprotein-complex-binding site of dystrophin. Three dystrophin-associated proteins bind directly to the carboxy-terminal portion of dystrophin. *Eur. J. Biochem./FEBS* **220,** 283–292
5. Bonilla, E., Samitt, C. E., Miranda, A. F., Hays, A. P., Salviati, G., DiMauro, S., Kunkel, L. M., Hoffman, E. P., and Rowland, L. P. (1988) Duchenne muscular dystrophy: deficiency of dystrophin at the muscle cell surface. *Cell* **54,** 447–452
6. Mauro, A. (1961) Satellite cell of skeletal muscle fibers. *J. Biophys. Biochem. Cytol.* **9,** 493–495
7. Moss, F. P., and Leblond, C. P. (1971) Satellite cells as the source of nuclei in muscles of growing rats. *Anat. Rec.* **170,** 421–435
8. Snow, M. H. (1978) An autoradiographic study of satellite cell differentiation into regenerating myotubes following transplantation of muscles in young rats. *Cell Tissue Res.* **186,** 535–540
9. Jejurikar, S. S., and Kuzon, W. M., Jr. (2003) Satellite cell depletion in degenerative skeletal muscle. *Apoptosis* **8,** 573–578
10. Schultz, E., and Jaryszak, D. L. (1985) Effects of skeletal muscle regeneration on the proliferation potential of satellite cells. *Mech. Ageing Dev.* **30,** 63–72
11. Webster, C., and Blau, H. M. (1990) Accelerated age-related decline in replicative life-span of Duchenne muscular dystrophy myoblasts: implications for cell and gene therapy. *Somat. Cell Mol. Genet.* **16,** 557–565
12. Hashimoto, N., Murase, T., Kondo, S., Okuda, A., and Inagawa-Ogashiwa, M. (2004) Muscle reconstitution by muscle satellite

cell descendants with stem cell-like properties. *Development (Camb.)* **131,** 5481–5490
13. Montarras, D., Morgan, J., Collins, C., Relaix, F., Zaffran, S., Cumano, A., Partridge, T., and Buckingham, M. (2005) Direct isolation of satellite cells for skeletal muscle regeneration. *Science* **309,** 2064–2067
14. Collins, C. A., Olsen, I., Zammit, P. S., Heslop, L., Petrie, A., Partridge, T. A., and Morgan, J. E. (2005) Stem cell function, self-renewal, and behavioral heterogeneity of cells from the adult muscle satellite cell niche. *Cell* **122,** 289–301
15. Partridge, T. A., Morgan, J. E., Coulton, G. R., Hoffman, E. P., and Kunkel, L. M. (1989) Conversion of mdx myofibres from dystrophin-negative to -positive by injection of normal myoblasts. *Nature* **337,** 176–179
16. Mendell, J. R., Kissel, J. T., Amato, A. A., King, W., Signore, L., Prior, T. W., Sahenk, Z., Benson, S., McAndrew, P. E., Rice, R., Nagaraja, H., Stephens, R., Lantry, L., Morris, G. E., and Burghes, A. H. M. (1995) Myoblast transfer in the treatment of Duchenne's muscular dystrophy. *N. Engl. J. Med.* **333,** 832–838
17. Weissman, I. L., Anderson, D. J., and Gage, F. (2001) Stem and progenitor cells: origins, phenotypes, lineage commitments, and transdifferentiations. *Annu. Rev. Cell Dev. Biol.* **17,** 387–403
18. Relaix, F., Montarras, D., Zaffran, S., Gayraud-Morel, B., Rocancourt, D., Tajbakhsh, S., Mansouri, A., Cumano, A., and Buckingham, M. (2006) Pax3 and Pax7 have distinct and overlapping functions in adult muscle progenitor cells. *J. Cell Biol.* **172,** 91–102
19. Seale, P., Sabourin, L. A., Girgis-Gabardo, A., Mansouri, A., Gruss, P., and Rudnicki, M. A. (2000) Pax7 is required for the specification of myogenic satellite cells. *Cell* **102,** 777–786
20. Cornelison, D. D., and Wold, B. J. (1997) Single-cell analysis of regulatory gene expression in quiescent and activated mouse skeletal muscle satellite cells. *Dev. Biol.* **191,** 270–283
21. Hollnagel, A., Grund, C., Franke, W. W., and Arnold, H. H. (2002) The cell adhesion molecule M-cadherin is not essential for muscle development and regeneration. *Mol. Cell. Biol.* **22,** 4760–4770
22. Bottaro, D. P., Rubin, J. S., Faletto, D. L., Chan, A. M., Kmiecik, T. E., Vande Woude, G. F., and Aaronson, S. A. (1991) Identification of the hepatocyte growth factor receptor as the c-met proto-oncogene product. *Science* **251,** 802–804
23. Fukada, S., Higuchi, S., Segawa, M., Koda, K., Yamamoto, Y., Tsujikawa, K., Kohama, Y., Uezumi, A., Imamura, M., Miyagoe-Suzuki, Y., Takeda, S., and Yamamoto, H. (2004) Purification and cell-surface marker characterization of quiescent satellite cells from murine skeletal muscle by a novel monoclonal antibody. *Exp. Cell Res.* **296,** 245–255
24. Dekel, I., Magal, Y., Pearson-White, S., Emerson, C. P., and Shani, M. (1992) Conditional conversion of ES cells to skeletal muscle by an exogenous MyoD1 gene. *New Biol.* **4,** 217–224
25. Rohwedel, J., Maltsev, V., Bober, E., Arnold, H. H., Hescheler, J., and Wobus, A. M. (1994) Muscle cell differentiation of embryonic stem cells reflects myogenesis in vivo: developmentally regulated expression of myogenic determination genes and functional expression of ionic currents. *Dev. Biol.* **164,** 87–101
26. Barberi, T., Bradbury, M., Dincer, Z., Panagiotakos, G., Socci, N. D., and Studer, L. (2007) Derivation of engraftable skeletal myoblasts from human embryonic stem cells. *Nat. Med.* **13,** 642–648
27. Doetschman, T. C., Eistetter, H., Katz, M., Schmidt, W., and Kemler, R. (1985) The in vitro development of blastocyst-derived embryonic stem cell lines: formation of visceral yolk sac, blood islands and myocardium. *J. Embryol. Exp. Morphol.* **87,** 27–45
28. Niwa, H., Yamamura, K., and Miyazaki, J. (1991) Efficient selection for high-expression transfectants with a novel eukaryotic vector. *Gene* **108,** 193–199
29. Yoshimoto, M., Chang, H., Shiota, M., Kobayashi, H., Umeda, K., Kawakami, A., Heike, T., and Nakahata, T. (2005) Two different roles of purified CD45+c-Kit+Sca-1+Lin-cells after transplantation in muscles. *Stem Cells (Dayton)* **23,** 610–618
30. Harris, J. B. (2003) Myotoxic phospholipases A2 and the regeneration of skeletal muscles. *Toxicon* **42,** 933–945
31. Fukada, S., Miyagoe-Suzuki, Y., Tsukihara, H., Yuasa, K., Higuchi, S., Ono, S., Tsujikawa, K., Takeda, S., and Yamamoto, H. (2002) Muscle regeneration by reconstitution with bone marrow or fetal liver cells from green fluorescent protein-gene transgenic mice. *J. Cell Sci.* **115,** 1285–1293
32. Gross, J. G., and Morgan, J. E. (1999) Muscle precursor cells injected into irradiated mdx mouse muscle persist after serial injury. *Muscle Nerve* **22,** 174–185
33. Rosenblatt, J. D., Lunt, A. I., Parry, D. J., and Partridge, T. A. (1995) Culturing satellite cells from living single muscle fiber explants. *In Vitro Cell. Dev. Biol.* **31,** 773–779
34. Dhawan, J., and Rando, T. A. (2005) Stem cells in postnatal myogenesis: molecular mechanisms of satellite cell quiescence, activation and replenishment. *Trends Cell Biol.* **15,** 666–673
35. Zammit, P. S., Relaix, F., Nagata, Y., Ruiz, A. P., Collins, C. A., Partridge, T. A., and Beauchamp, J. R. (2006) Pax7 and myogenic progression in skeletal muscle satellite cells. *J. Cell Sci.* **119,** 1824–1832
36. Relaix, F., Rocancourt, D., Mansouri, A., and Buckingham, M. (2005) A Pax3/Pax7-dependent population of skeletal muscle progenitor cells. *Nature* **435,** 948–953
37. Tajbakhsh, S., Rocancourt, D., Cossu, G., and Buckingham, M. (1997) Redefining the genetic hierarchies controlling skeletal myogenesis: Pax-3 and Myf-5 act upstream of MyoD. *Cell* **89,** 127–138
38. Kiefer, J. C., and Hauschka, S. D. (2001) Myf-5 is transiently expressed in nonmuscle mesoderm and exhibits dynamic regional changes within the presegmented mesoderm and somites I-IV. *Dev. Biol.* **232,** 77–90
39. Hirsinger, E., Malapert, P., Dubrulle, J., Delfini, M. C., Duprez, D., Henrique, D., Ish-Horowicz, D., and Pourquie, O. (2001) Notch signalling acts in postmitotic avian myogenic cells to control MyoD activation. *Development (Camb.)* **128,** 107–116
40. Smith, T. H., Block, N. E., Rhodes, S. J., Konieczny, S. F., and Miller, J. B. (1993) A unique pattern of expression of the four muscle regulatory factor proteins distinguishes somitic from embryonic, fetal and newborn mouse myogenic cells. *Development (Camb.)* **117,** 1125–1133
41. Kassar-Duchossoy, L., Giacone, E., Gayraud-Morel, B., Jory, A., Gomes, D., and Tajbakhsh, S. (2005) Pax3/Pax7 mark a novel population of primitive myogenic cells during development. *Genes Dev.* **19,** 1426–1431
42. Harrison, D. E., Astle, C. M., and Delaittre, J. A. (1978) Loss of proliferative capacity in immunohemopoietic stem cells caused by serial transplantation rather than aging. *J. Exp. Med.* **147,** 1526–1531
43. Yao, S. N., and Kurachi, K. (1993) Implanted myoblasts not only fuse with myofibers but also survive as muscle precursor cells. *J. Cell Sci.* **105**(Pt. 4), 957–963
44. Rando, T. A., and Blau, H. M. (1994) Primary mouse myoblast purification, characterization, and transplantation for cell-mediated gene therapy. *J. Cell Biol.* **125,** 1275–1287
45. Sherwood, R. I., Christensen, J. L., Conboy, I. M., Conboy, M. J., Rando, T. A., Weissman, I. L., and Wagers, A. J. (2004) Isolation of adult mouse myogenic progenitors: functional heterogeneity of cells within and engrafting skeletal muscle. *Cell* **119,** 543–554
46. Darabi, R., Gehlbach, K., Bachoo, R. M., Kamath, S., Osawa, M., Kamm, K. E., Kyba, M., and Perlingeiro, R. C. (2008) Functional skeletal muscle regeneration from differentiating embryonic stem cells. *Nat. Med.* **14,** 134–143

Received for publication October 21, 2008.
Accepted for publication January 8, 2009.

Immunity
Resource

Functional Delineation and Differentiation Dynamics of Human CD4$^+$ T Cells Expressing the FoxP3 Transcription Factor

Makoto Miyara,[1,10] Yumiko Yoshioka,[1,9] Akihiko Kitoh,[1,9] Tomoko Shima,[1,9] Kajsa Wing,[1] Akira Niwa,[2] Christophe Parizot,[3] Cécile Taflin,[3] Toshio Heike,[2] Dominique Valeyre,[4] Alexis Mathian,[3] Tatsutoshi Nakahata,[2] Tomoyuki Yamaguchi,[1] Takashi Nomura,[1] Masahiro Ono,[1] Zahir Amoura,[5,6] Guy Gorochov,[3,6] and Shimon Sakaguchi[1,7,8,*]

[1]Department of Experimental Pathology, Institute for Frontier Medical Sciences
[2]Department of Pediatrics, Graduate School of Medicine
Kyoto University, Kyoto 606-8507, Japan
[3]Institut National de la Santé et de la Recherche Médicale (INSERM) UMR-S 945, Laboratoire AP-HP d'immunologie cellulaire et tissulaire, Hôpital Pitié-Salpêtrière, 75013 Paris, France
[4]Pneumology Department, AP-HP Hôpital Avicenne, 93000 Bobigny, France
[5]Internal Medicine Department, AP-HP Hôpital Pitié-Salpêtrière, 75013 Paris, France
[6]Pierre and Marie Curie University, UPMC Paris Universitas, 75005 Paris, France
[7]Core Research for Evolutional Science and Technology (CREST), Japan Science and Technology Agency, Kawaguchi 332-0012, Japan
[8]WPI Immunology Frontier Research Center, Osaka University, Suita 565-0871, Japan
[9]These authors contributed equally to this work
[10]Present address: Internal Medicine Department and Institut National de la Santé et de la Recherche Médicale (INSERM) UMR-S 945, Laboratoire AP-HP d'immunologie cellulaire et tissulaire, Hôpital Pitié-Salpêtrière, 75013 Paris, France
*Correspondence: shimon@frontier.kyoto-u.ac.jp
DOI 10.1016/j.immuni.2009.03.019

SUMMARY

FoxP3 is a key transcription factor for the development and function of natural CD4$^+$ regulatory T cells (Treg cells). Here we show that human FoxP3$^+$CD4$^+$ T cells were composed of three phenotypically and functionally distinct subpopulations: CD45RA$^+$FoxP3^{lo} resting Treg cells (rTreg cells) and CD45RA$^-$FoxP3^{hi} activated Treg cells (aTreg cells), both of which were suppressive in vitro, and cytokine-secreting CD45RA$^-$FoxP3^{lo} nonsuppressive T cells. The proportion of the three subpopulations differed between cord blood, aged individuals, and patients with immunological diseases. Terminally differentiated aTreg cells rapidly died whereas rTreg cells proliferated and converted into aTreg cells in vitro and in vivo. This was shown by the transfer of rTreg cells into NOD-scid-common γ-chain-deficient mice and by TCR sequence-based T cell clonotype tracing in peripheral blood in a normal individual. Taken together, the dissection of FoxP3$^+$ cells into subsets enables one to analyze Treg cell differentiation dynamics and interactions in normal and disease states, and to control immune responses through manipulating particular FoxP3$^+$ subpopulations.

INTRODUCTION

FoxP3-expressing CD4$^+$ thymus-derived naturally occurring regulatory T cells (Treg cells) play an indispensable role for the maintenance of self tolerance and immune homeostasis (Sakaguchi et al., 2008). They play crucial roles in human diseases, such as autoimmune disease, allergy, and cancer (Curiel et al., 2004; Ehrenstein et al., 2004; Kriegel et al., 2004; Miyara et al., 2005; Viglietta et al., 2004). Human natural Treg cells were initially defined according to their high expression of CD25 (Baecher-Allan et al., 2001; Dieckmann et al., 2001; Jonuleit et al., 2001; Levings et al., 2001; Ng et al., 2001; Taams et al., 2001), based on the finding that murine CD25$^+$CD4$^+$ T cells are highly suppressive (Sakaguchi et al., 1995). With the discovery of FoxP3 as a "master control gene" for CD4$^+$ Treg cell development and function (Fontenot et al., 2003; Hori et al., 2003; Khattri et al., 2003), detection of FoxP3 at the mRNA and protein level revealed that human CD25^{hi}CD4$^+$ T cells indeed express FoxP3 (Miyara et al., 2006; Roncador et al., 2005; Yagi et al., 2004). In contrast to murine FoxP3$^+$ Treg cells, however, human FoxP3$^+$ cells may not be functionally homogenous. For example, it has been reported that mere TCR stimulation can induce FoxP3 expression in apparently naive human FoxP3$^-$CD4$^+$ T cells without conferring suppressive activity (Allan et al., 2007; Gavin et al., 2006; Tran et al., 2007; Wang et al., 2007). Furthermore, some FoxP3$^+$ cells are phenotypically naive (e.g., CD45RA$^+$), present in cord blood as well as in peripheral blood of adults, and suppressive in vitro (Valmori et al., 2005), whereas other FoxP3$^+$ cells phenotypically resemble memory T cells (e.g., CD45RA$^-$) and are suggested to originate from peripheral memory FoxP3$^-$CD4$^+$ T cells (Vukmanovic-Stejic et al., 2006). To better understand the roles of FoxP3$^+$ T cells for the control of immune responses, it is necessary to determine whether FoxP3-expressing T cells in freshly isolated CD4$^+$ T cells are functionally heterogeneous, how functionally different subpopulations of FoxP3$^+$ cells can be reliably delineated, and how such

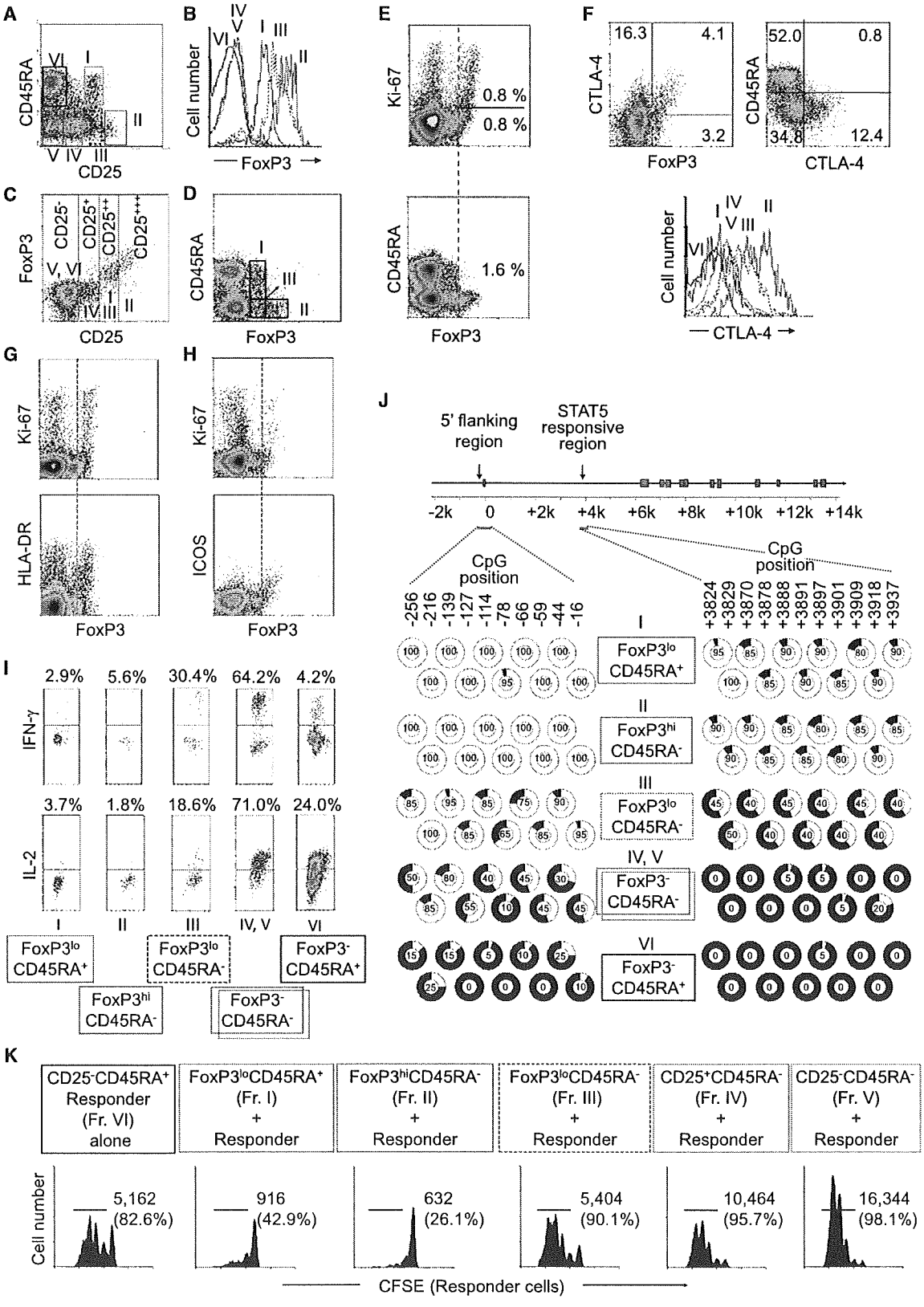
A
CD45RA
CD25
B
Cell number
FoxP3
C
FoxP3
CD25
D
CD45RA
FoxP3
E
Ki-67
0.8 %
0.8 %
CD45RA
1.6 %
FoxP3
F
CTLA-4
FoxP3
16.3
4.1
3.2
CD45RA
CTLA-4
52.0
0.8
34.8
12.4
Cell number
CTLA-4
G
Ki-67
HLA-DR
FoxP3
H
Ki-67
ICOS
FoxP3
I
IFN-γ
IL-2
2.9%
5.6%
30.4%
64.2%
4.2%
3.7%
1.8%
18.6%
71.0%
24.0%
I
II
III
IV, V
VI
FoxP3lo CD45RA+
FoxP3hi CD45RA-
FoxP3lo CD45RA-
FoxP3- CD45RA-
FoxP3- CD45RA+
J
5' flanking region
STAT5 responsive region
-2k
0
+2k
+4k
+6k
+8k
+10k
+12k
+14k
CpG position
-256 -216 -139 -127 -114 -78 -66 -59 -44 -16
+3824 +3829 +3870 +3878 +3888 +3891 +3897 +3901 +3909 +3918 +3937
I
FoxP3lo CD45RA+
II
FoxP3hi CD45RA-
III
FoxP3lo CD45RA-
IV, V
FoxP3- CD45RA-
VI
FoxP3- CD45RA+
K
CD25-CD45RA+ Responder (Fr. VI) alone
FoxP3loCD45RA+ (Fr. I) + Responder
FoxP3hiCD45RA- (Fr. II) + Responder
FoxP3loCD45RA- (Fr. III) + Responder
CD25+CD45RA- (Fr. IV) + Responder
CD25-CD45RA- (Fr. V) + Responder
Cell number
5,162 (82.6%)
916 (42.9%)
632 (26.1%)
5,404 (90.1%)
10,464 (95.7%)
16,344 (98.1%)
CFSE (Responder cells)

subsets differentiate and interact in physiological and disease states.

In this report, we show that human FoxP3+CD4+ T cells can be separated into three functionally and phenotypically different subpopulations based on the expression of FoxP3, cell surface phenotype, the degree of DNA methylation of the FoxP3 gene, DNA microarray profile, proliferation status in the physiological state, cytokine secreting capacity, TCR repertoire, and in vitro suppressive activity. These populations are (1) CD45RA+FoxP3lo resting Treg cells, (2) CD45RA−FoxP3hi activated Treg cells, and (3) cytokine-secreting CD45RA−FoxP3lo non-Treg cells. With this dissection of FoxP3+ T cells into subpopulations, we show the dynamics of Treg cell differentiation in vitro, in vivo, and ex vivo in normal and disease states. The results indicate that functional and numerical analysis of each FoxP3+ subset is essential for assessing immunological states, and that manipulation of a particular subset, rather than whole FoxP3+ cells, helps to dampen or augment a variety of physiological and pathological immune responses.

RESULTS

Separation of FoxP3+CD4+ T Cells into Three Subpopulations by the Expression of FoxP3, CD25, and CD45RA

The combination of CD25 and CD45RA staining of CD4+ T cells in peripheral blood lymphocytes (PBL) of normal healthy individuals revealed six subpopulations (Fraction [Fr.] I–VI) that expressed the FoxP3 protein at different amounts (Figures 1A and 1B). Among them, Fr. I, II, and III were FoxP3+ (Figure 1B) and the degree of FoxP3 expression in these fractions were proportional to CD25 expression (Figure 1C). Notably, these three FoxP3+ populations could be distinctly separated by the combination of FoxP3 and CD45RA staining; i.e., FoxP3loCD45RA+ cells, which were CD25++ (Fr. I), FoxP3hiCD45RA− cells, which were CD25+++ (Fr. II), and FoxP3loCD45RA− cells, which were CD25++ (Fr. III) (Figure 1D). The fractions could be prepared as live cells by cell sorting as CD25++CD45RA+, CD25+++CD45RA−, and CD25++CD45RA− cells, respectively (Figure S1A available online). Purified Fr. I, II, and III populations expressed FoxP3 transcripts to a similar degree irrespective of different amounts of FoxP3 protein expressed in each population (Figure 1B; Figure S1B). Fr. IV formed a distinct population as CD25+FoxP3− cells (Figure 1C), but it was not well demarcated from Fr. V by CD45RA or CD25 staining (Figure 1A). Therefore, we analyzed Fr. IV and V together in the functional examination of FoxP3+ subsets (see below).

Assessment of the proliferative status of each subpopulation in the physiological state by detecting the expression of Ki-67, a nuclear protein expressed in cells ready to proliferate and at a higher amount in actually proliferating cells (Figure S2), revealed that about half of the cells in Fr. II were proliferating whereas the cells in Fr. I and III were not (red dotted line in Figure 1E). Fr. II expressed intracellular CTLA-4 to the highest degree whereas Fr. I hardly expressed the molecule (Figure 1F). Furthermore, Fr. II corresponded to HLA-DR-expressing and also ICOS-expressing FoxP3+ cells as reported by others (Figures 1G and 1H; Baecher-Allan et al., 2006; Ito et al., 2008).

Analysis of cytokine production by each fraction showed that Fr. II scarcely produced IL-2 or IFN-γ. Among FoxP3lo cells, Fr. I was poor producer of IL-2 and IFN-γ whereas Fr. III produced high amounts of these cytokines (Figure 1I; Figure S3).

The 5′ flanking region and a STAT5-responsive region in the intron 1 of the *FOXP3* gene are critical for induction and enhancement of FoxP3 expression by TCR and IL-2 stimulation (Floess et al., 2007; Mantel et al., 2006; Zorn et al., 2006). Analysis of the DNA methylation status of these regions in each fraction prepared from a male donor showed that the CpG methylation sites in the regions were completely demethylated in Fr. I and Fr. II (Figure 1J). The 5′ flanking region of Fr. III was also highly demethylated, although the demethylation pattern was less uniform compared with Fr. I and II. In contrast, their STAT5-responsive region was less demethylated than other FoxP3+ subsets. In addition, memory-like CD25+ and CD25− CD45RA−CD4+ non-Treg cells (Fr. IV, V), which were FoxP3−, had their 5′ flanking region moderately demethylated whereas the STAT5 responsive region was virtually completely methylated. Both regions were highly methylated in naive Fr. VI. These findings were confirmed by analysis of individual clones isolated from each subpopulation (Figure S4). The results collectively

Figure 1. Delineation of FoxP3+CD4+ T Cells into Subsets by Cell Surface Molecules, Proliferative State, Cytokine Production, Methylation Status of the *FOXP3* Gene, and In Vitro Suppressive Activity

(A–D) Six subsets of CD4+ T cells defined by the expression of CD45RA and CD25: pink line (Fraction [Fr.] I), CD25++CD45RA+ cells; bold red line (Fr. II), CD25+++CD45RA− cells; broken brown line (Fr. III), CD25++CD45RA− cells; green line (Fr. IV), CD25+CD45RA− cells; blue line (Fr. V), CD25−CD45RA− cells; black line (Fr. VI), CD25−CD45RA+ cells. Expression of FoxP3 (B), CD25 and intracellular FoxP3 (C), and CD45RA and FoxP3 (D) in each fraction shown in (A). Data are representative of 19 blood donors.

(E) Flow cytometry of the expression of nuclear Ki-67 and FoxP3 in CD4+ T cells. Red broken line separates Ki-67+FoxP3hi from Ki-67−FoxP3lo cells and CD45RA+FoxP3lo from CD45RA−FoxP3hi cells. The percentages of Ki-67+ and Ki-67−FoxP3hi cells among CD4+ cells are indicated in the top panel and the percentage of FoxP3hiCD45RA− cells in the bottom panel.

(F) Flow cytometry of the expression of intracellular CTLA-4 and FoxP3 (top left); CD45RA and CTLA-4 (top right) by CD4+ T cells; and expression of CTLA-4 by each fraction defined in (A)–(D) (bottom). Numbers indicate percent of cells in each quadrant.

(G and H) Expression of Ki-67 and FoxP3 (top) and of HLA-DR or ICOS and FoxP3 (bottom). Red broken line separates Ki-67+FoxP3hi from Ki-67−FoxP3lo cells and HLA-DR−FoxP3lo from HLA-DR+FoxP3hi cells (G) or ICOS−FoxP3lo from ICOS+FoxP3hi cells (H).

(I) Production of IFN-γ, IL-2 by each fraction after stimulation with PMA + ionomycin, and percent of cytokine-secreting cells in each fraction is shown. Data are representative of six independent experiments.

(J) Analysis of DNA methylation status at 5′ flanking region (left) and STAT5-responsive (right) region of the *FOXP3* gene in FoxP3-expressing or -nonexpressing CD4+ T cell subsets (Figure S1) from PBMCs of one healthy male donor. Percentages of clones displaying demethylation of indicated CpG methylation sites are indicated and depicted in white in sector graphs. 19 to 20 clones were sequenced from each CD4+ T cell subset.

(K) CFSE dilution by 10^4 labeled CD25−CD45RA+CD4+ responder T cells assessed after 84–90 hr of TCR-stimulated coculture with indicated CD4+ T cell subset at a 1 to 1 ratio. Cell number and percentage of dividing cells per well are indicated. Data are representative of 12 separate experiments.

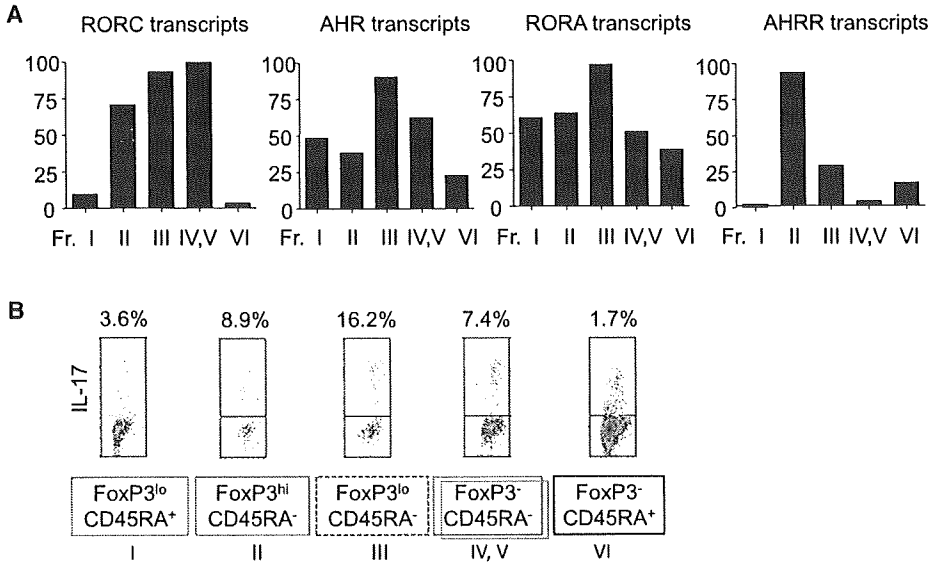

Figure 2. CD45RA⁻FoxP3^{lo}CD4⁺ T Cells Contain Cells with Th17 Cell Potential

(A) The amounts of transcripts of indicated genes in separated CD4⁺ T cell subsets were assessed by quantitative PCR.

(B) Flow cytometry of the production of IL-17 by gated CD4⁺ T cell subsets after stimulation with PMA + ionomycin for 5 hr. Percentages of cytokine-secreting cells are shown. Data are representative of six independent experiments.

indicate that Fr. I and II are active in FoxP3 gene transcription and close in their differentiation stage, and that, compared with these fractions, Fr. III may be less capable of maintaining FoxP3 expression in the presence of IL-2 and STAT5 signaling.

To assess the in vitro suppressive potency of each fraction, we measured the extent of CFSE dilution of labeled naive CD25⁻CD45RA⁺CD4⁺ T cells (hereafter called responder cells) cocultured with an equal number of each fraction and stimulated for 4 days (Figure 1K). Fr. I and II (isolated as CD25^{++}CD45RA⁺ and CD25^{+++}CD45RA⁻ cells, respectively, as shown in Figure S1) potently suppressed the proliferation of responder cells, whereas Fr. III, IV, and V did not and even enhanced the responder proliferation. The inability of Fr. III (CD45RA⁻Foxp3^{lo} cells) to suppress was confirmed by using CD127 as an additional marker for purifying FoxP3-expressing cells from CD4⁺ T cells (Figure S5; Liu et al., 2006; Seddiki et al., 2006).

Taken together, three distinct subpopulations of FoxP3⁺CD4⁺ T cells can be defined in human PBL by the expression of CD45RA and FoxP3 as summarized in Table S1; i.e., Fr. I: CTLA-4^{lo}Ki-67⁻CD45RA⁺FoxP3^{lo} T cells; Fr. II: CTLA-4^{hi}CD45RA⁻FoxP3^{hi} cells, both of which possess a fully functional *FOXP3* gene, hardly secrete cytokines, and potently suppress proliferation; and Fr. III: CTLA-4^{int}CD45RA⁻FoxP3^{lo} T cells, which secrete cytokines, are much less active in the expression of the *FOXP3* gene under the control via STAT5, and do not suppress proliferation in vitro. Based on their phenotypic and functional characteristics, Fr. I and Fr. II can be designated as resting Treg cells (rTreg cells) and activated Treg cells (aTreg cells), respectively.

FoxP3^{lo}CD45RA⁻ Nonregulatory T Cells Contain Cells with Th17 Cell Potential

DNA microarray analysis of each fraction showed that the gene expression patterns in the three FoxP3-expressing subpopulations were distinct (Figure S6A). Quantitative assessment of mRNA expression of differentially expressed genes revealed that the expression of RORC, a key transcription factor in Th17 cell lineage (Ivanov et al., 2006), was highly upregulated in Fr. II and III, indicating that RORC-FoxP3 double-positive population, which was recently described in mice (Yang et al., 2008a; Zhou et al., 2008), exists in humans as well in Fr. II and III (Figure S6B). Transcripts encoding RORα and AHR, both of which contribute to Th17 cell differentiation in mice (Veldhoen et al., 2008; Yang et al., 2008b), were highly upregulated in Fr.III, further indicating that this population contains cells with Th17 cell potential (Figure 2A). Also of note is that Fr. II specifically expressed high amounts of AHR repressor transcripts, suggesting that Treg cell differentiation might accompany an inhibition of Th17 cell differentiation via expression of AHR repressor. Assessment of cytokine production revealed that Fr. III was the highest producer of IL-17 even compared with naive FoxP3⁻CD45RA⁺ (Fr. VI) or memory-like FoxP3⁻CD45RA⁻CD4⁺ non-Treg cells (Fr. IV and V) (Figure 2B; Figure S3).

Thus, DNA microarray profiling of FoxP3⁺ subpopulations supports the relevance of separating FoxP3⁺CD4⁺ T cells into three subsets. Further, regarding the cell lineage relationship of FoxP3⁺ cells and Th17 cells, Fr. III contains FoxP3-RORγ double-positive cells with a Th17 cell potential, in addition to IL-2- and/or IFN-γ-producing cells (Figure 1I).

Resting Treg Cells Proliferate whereas Activated Treg Cells Die while Suppressing In Vitro

As shown in Figure 1E, fresh Fr. I cells (rTreg cells) did not express Ki-67. However, when they were cocultured with responder cells and TCR stimulated, all the FoxP3-expressing cells became Ki-67⁺ on day 4, indicating that rTreg cells proliferate (Figure S7). Assessment of proliferation by CFSE dilution during 4 days of culture also revealed that both aTreg cells

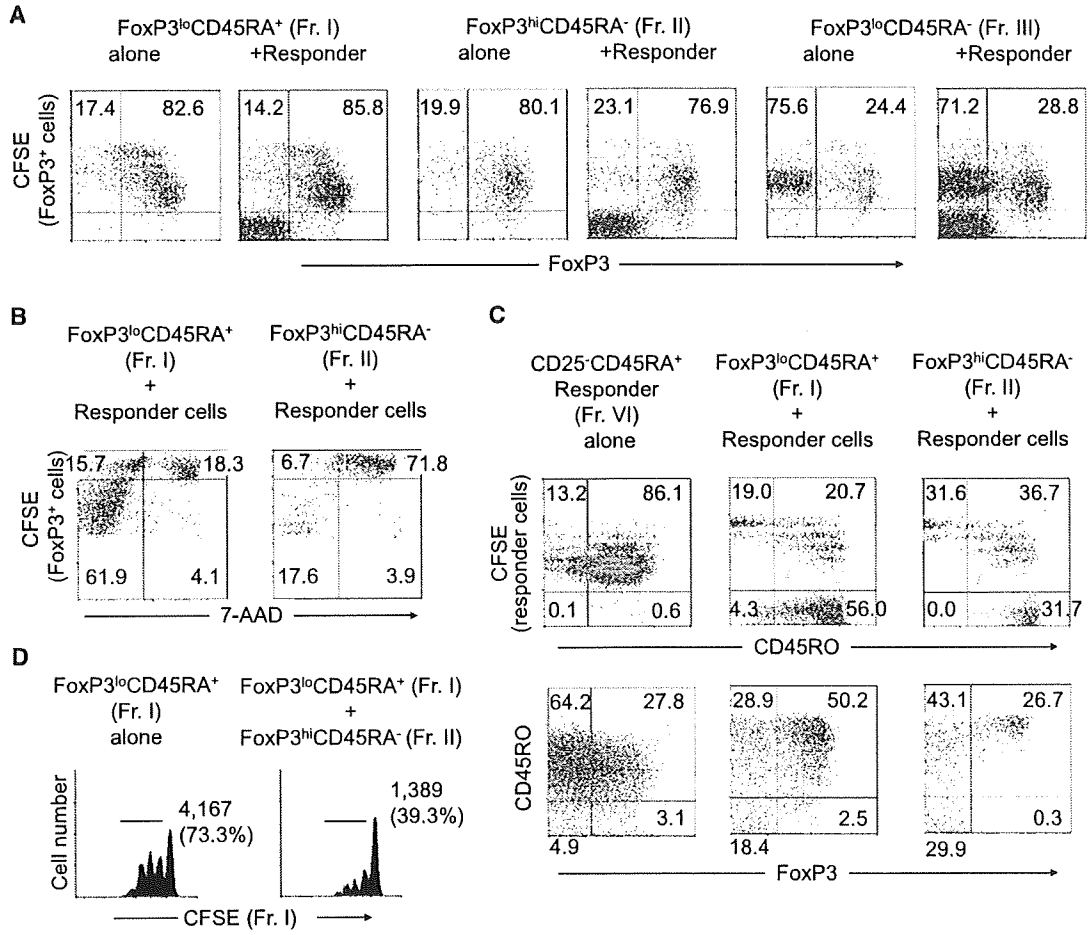

Figure 3. In Vitro Properties of FoxP3+ Subpopulations

(A) CFSE dilution by rTreg or aTreg cells and intracellular expression of FoxP3 were analyzed after 4 days TCR stimulation in the absence or presence of nonlabeled responder cells. Percentages of FoxP3$^-$ and of FoxP3$^+$ cells among CFSE-labeled cells are indicated.

(B) Viability assessed by 7-AAD staining of CFSE-labeled CD45RA$^+$FoxP3^{lo} (left) or CD45RA$^-$FoxP3^{hi} Treg cells (right) cocultured with nonlabeled responder cells for 4 days. Only CFSE-labeled cells are shown. Numbers indicate percentage in each quadrant. Data shown are representative of five independent experiments.

(C) CFSE dilution, surface CD45RO, and intracellular FoxP3 expression by CFSE-labeled responder cells cultured alone or cocultured with unlabeled Treg cell subsets for 4 days. Numbers indicate percentage in each quadrant.

(D) CFSE dilution of labeled rTreg cells cultured alone or with aTreg cells at a 1 to 1 ratio. Numbers and percentage of proliferating cells are indicated. Data shown in (B) and (D) are representative of five independent experiments.

(Fr. II) and rTreg cells (Fr. I) gave rise to CFSE-diluting FoxP3$^+$ cells when cultured alone (Figure 3A). In addition, rTreg cells showed more active proliferation than did aTreg cells in the presence of responder cells. In contrast with rTreg or aTreg cells, most (~70%) of CD45RA$^-$FoxP3^{lo}CD4$^+$ T cells (Fr. III) did not express FoxP3 during their proliferation, indicating that FoxP3 expression in the majority of Fr. III cells may not be stable in concordance with the methylation status of their *FOXP3* gene (Figure 3A).

Based on the finding that very few aTreg cells (Fr. II) were detectable after 4 days of culture (Figure S7), we assessed the viability of Treg cells by measuring incorporation of 7-AAD by CFSE-labeled rTreg or aTreg cells cultured with responder cells (Figure 3B). The majority (~75%) of aTreg cells were positive for 7-AAD. By contrast, although a fraction (~20%) of rTreg cells were nonproliferative and 7-AAD$^+$, the majority of proliferating rTreg cells (~60%) were 7-AAD$^-$ (Figure 3B). In addition to proliferation, rTreg cells showed increased expression of FoxP3 (Figure 3A), CD45RO (Figure 3C), and intracellular CTLA-4 (Figure S8). High expression of CD45RO was secondary to activation because rTreg cells, which were CD45RA$^+$, did not express CD45RO when freshly isolated from peripheral blood (Figure S9). Further, when CFSE-labeled rTreg cells (Fr. I) were cultured with nonlabeled aTreg cells (Fr. II), the latter substantially suppressed the proliferation of the former (Figure 3D).

Taken together, rTreg cells are not anergic and are able to proliferate upon TCR stimulation. They acquire a Ki-67$^+$FoxP3^{hi} aTreg cell phenotype and exert suppression during and after their proliferation and conversion to aTreg cells, which die after proliferation and exertion of suppression. Activated Treg cells also suppress the proliferation of resting Treg cells in a negative feedback fashion. Thus, in addition to different cell surface phenotypes, rTreg and aTreg cells possess different cell fates despite their comparable in vitro suppressive activity when assessed separately.

In Vivo Conversion of rTreg Cells to aTreg Cells and Differentiation of a Small Fraction of FoxP3$^-$ Cells to FoxP3$^+$ Cells

Next, to investigate whether the in vitro conversion of rTreg cells to aTreg cells could also occur in vivo, we transferred human PBMCs containing CFSE-labeled CD4$^+$ T cells into NOG (Nod-scid-common γ-chain-deficient) mice and analyzed their splenocytes 5 days after transfer (Hiramatsu et al., 2003). FoxP3^{hi}CD4$^+$ T cells recovered in the recipients were largely CD25^{hi} and CD45RO$^+$ (data not shown) and mostly confined to Ki-67$^+$CFSE-diluting cells, which had divided more than 6 times after transfer (Figure 4A). In addition, most CD4$^+$ T cells expressing low amounts of FoxP3 had not proliferated. These findings correspond to the in vitro findings that FoxP3^{hi} aTreg cells found in PBMCs were highly proliferative and that FoxP3^{lo}CD4$^+$ T cells were Ki-67$^-$ in PBMCs (Figure 1E), suggesting that, upon activation, rTreg cells upregulate FoxP3 expression and then proliferate. We also examined the behavior of Treg cells or whole FoxP3$^+$ cells when injected without other effector CD4$^+$ T cells. Neither population proliferated, indicating that the maintenance and proliferation of FoxP3-expressing cells requires the presence of other CD4$^+$ T cells in vivo (Figure S10).

Similar analysis of PBMCs containing CFSE-labeled rTreg cells, prepared as shown in Figure 1A and Figure S1, showed that they proliferated in vivo and upregulated the expression of FoxP3 and CD45RO along several cell divisions (Figure 4B and data not shown). Because most FoxP3^{hi} cells were detected in CFSE-negative cells after transfer of CFSE-labeled CD4$^+$ T cells or rTreg cells (Figures 4A and 4B), we attempted to determine whether rTreg cells were the major source of CFSE-negative FoxP3^{hi} cells. Injection of PBMCs containing CFSE-labeled CD4$^+$ T cells devoid of rTreg cells revealed a much lower number of FoxP3^{hi} cells when compared with injection of whole CD4$^+$ T cells, indicating that most FoxP3^{hi} aTreg cells derive from rTreg cells (Figure 4C).

Further, to investigate whether the conversion of FoxP3$^-$ to FoxP3$^+$ in CD4$^+$ T cells could occur in vivo, we transferred PBMCs containing CFSE-labeled FoxP3$^-$ CD127^{hi}CD4$^+$ T cells together with nonlabeled FoxP3$^+$ cells (as CD25^{hi}CD127^{lo} cells) in NOG mice and examined whether FoxP3$^-$CD4$^+$ T cells could upregulate FoxP3 in vivo (Figure 4D). Although most CFSE-labeled cells remained FoxP3$^-$, a small number of cells upregulated FoxP3 from low to high amounts. Injection of only CFSE-labeled CD4$^+$FoxP3$^-$ cells confirmed that a small fraction (<1%) of CD4$^+$FoxP3$^-$ cells indeed divided at least 6 times to give rise to FoxP3^{hi} cells (Figure 4E). Taken together, these results indicate that rTreg cells convert to aTreg cells and that only a small fraction of aTreg cells derives from FoxP3$^-$CD4$^+$ non-Treg cells in vivo.

In Vivo Conversion of rTreg Cells to aTreg Cells in a Normal Human Individual

To obtain further evidence for the in vivo rTreg to aTreg cell conversion in normal humans, we attempted to trace clonotypes of each Treg cell fraction in a single individual at separate time points. Cells in rTreg cells (Fr. I), aTreg cells (Fr. II), and also FoxP3$^-$ non-Treg CD4$^+$ T cells (Fr. IV, V, VI) that expressed the same TCRBV5 family were sorted from a single healthy individual at 18 month intervals. Single-cell RT-PCR and DNA sequencing of the amplicons was performed to compare TCRBV5 CDR3 regions in each sorted subset. Given the small size of the sample, the analysis was able to monitor dominant clones only. First, we observed that rTreg (Fr. I) and aTreg (Fr. II) cell subsets shared few dominant clonotypes at a given time point. Second, we found that a clonotype initially detected in the rTreg cell subset was found dominant 18 months later in the aTreg but not in the rTreg cell subset. The TCR repertoire being potentially so heterogeneous and the sample size being so limited (45 to 137 cells analyzed in each subset), it is highly improbable that T cell clones with identical TCR sequences could be found in the same subsets only by chance. Indeed, when random samples of conventional CD4$^+$ T cells were similarly compared, shared clonotypes were never found in this individual (Figure 5; Table S2). The analysis also revealed that none of the clonotypes found in FoxP3$^-$ cells was found in aTreg cells 18 months later, indicating that if conversion of FoxP3$^-$CD4$^+$ T cells ever occurs in vivo, it may not be a frequent phenomenon compared with the conversion of rTreg cells to aTreg cells (Figure 5).

Based on these observations in Figures 4 and 5, we conclude that most FoxP3^{hi} aTreg cells are derived from recently activated and vigorously proliferating rTreg cells, and that only a minority of aTreg cells can develop from FoxP3$^-$CD4$^+$ non-Treg cells in vivo. The result also indicates that the TCR repertoire of Treg cells, in particular that of aTreg cells, adaptively changes in normal individuals.

Variations in Human rTreg and aTreg Cell Populations under Normal and Disease Conditions

We then attempted to determine whether the dissection of FoxP3$^+$ T cells in adult humans into Fr. I–III based on CD45RA and FoxP3 expression was pertinent to the analysis of the dynamics of Treg cell generation and differentiation in ontogeny, aging, and disease states.

Although rTreg cells were highly prevalent in cord blood, we could easily detect Ki-67$^+$FoxP3^{hi}CD45RA$^-$CD4$^+$ T cells that corresponded to aTreg cells in adults. We failed to confirm the previously reported finding that all CD25$^+$CD4$^+$ T cells were FoxP3$^+$ in cord blood (Fritzsching et al., 2006). However, CD4$^+$ T cells expressing the highest amounts of CD25 contained only FoxP3$^+$ cells and CD127 expression efficiently separated FoxP3$^+$CD25$^+$ from FoxP3$^-$CD25$^+$CD4$^+$ T cells (Figure 6A). IFN-γ production was barely detectable in whole CD4$^+$ T cells whereas IL-2 production was observed in FoxP3^{lo}CD45RA$^-$CD4$^+$ T cells as in adults (data not shown).

Analysis of the expression of CD31 (PECAM-1), which is known to be expressed in recent thymic emigrants but lost during their post-thymic peripheral expansion (Kimmig et al., 2002), revealed that almost all CD31$^+$FoxP3$^+$CD4$^+$ T cells in adult PBL were confined in the CD45RA$^+$FoxP3^{lo} population (Fr. I). This finding suggests that the majority of rTreg cells may be recently derived from the thymus (Figure 6B).

The proportion of rTreg cells (Fr. I) among CD4$^+$ T cells was decreased in aged donors (1.1% ± 0.59%, n = 12 versus 2.40% ± 0.89% in healthy donors, n = 29; $p < 0.0001$) whereas that of aTreg cells (Fr. II) was increased (2.48% ± 1.07% versus 1.63% ± 0.53%; $p = 0.01$; Figures 6C and 6D).

We next applied our new definition of FoxP3$^+$ T cell subsets to the analysis of two pathological conditions that reportedly show

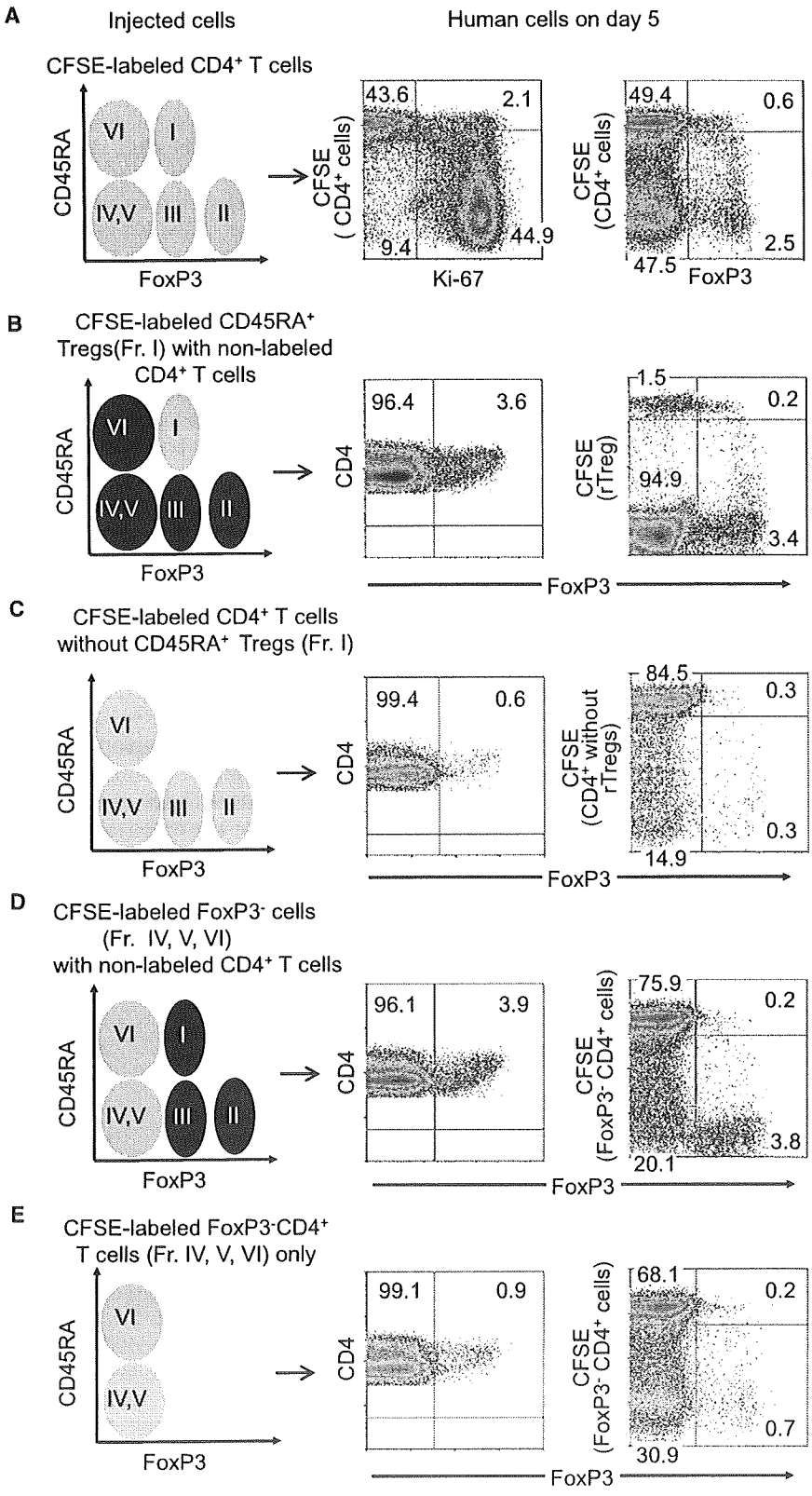

Figure 4. In Vivo Conversion of Treg Cell Phenotype in NOG Mice

PBMCs containing human CD4+ T cells were i.v. injected in NOG mice and collected in the spleen 5 days later. In schematic representations (left) of flow cytometric profiles of injected cells before transfer, CFSE-labeled CD4+ T subsets are depicted in green and injected with nonlabeled cells in black. Flow cytometry of human CD4+ T cells in the spleen after transfer of PBMCs containing CFSE-labeled human whole CD4+ T cells (A) or indicated CFSE-labeled CD4+ T cell subpopulations (B–E) into NOG mice. Numbers indicate percentage in each quadrant (right). Representative data of four mice transferred with PBMCs containing CFSE-labeled CD4+ T cells isolated from three different donors (A), and mice (two for each condition) transferred with PBMCs with indicated CFSE-labeled T cell populations obtained from two different donors (B–E).

different patterns of Treg cell involvement (Miyara et al., 2005, 2006). In sarcoidosis, a granulomatous disease of unknown origin, patients with active disease showed a considerable increase in the proportion of aTreg cells among CD4+ T cells (4.67% ± 3.35%, n = 41; $p < 0.0001$) combined with a high prevalence of Ki-67+FoxP3^{hi}CD4+ T cells and a decrease in the proportions of rTreg cells (1.48% ± 0.89%; $p < 0.0001$). In active systemic lupus erythematosus (SLE), a prototype of systemic autoimmune disease, there was a decrease in the proportion of aTreg cells (1.24 ± 0.72; n = 15; $p = 0.006$) and an increase in the proportions of rTreg cells (4.2 ± 1.86; $p = 0.0008$). Notably, CD45RA$^-$FoxP3^{lo} non-Treg cell fraction (Fr. III) increased to form a distinct population in active SLE (10.37% ± 9.3% versus 3.04 ± 1.1 in healthy donors; $p < 0.0001$; Figures 6C and 6D).

Thus, distinction of Treg cell subsets simply based on the combination of CD45RA and FoxP3 expression is highly informative in assessing the dynamics of Treg cell differentiation under physiological and disease conditions.

DISCUSSION

We have shown in this report that FoxP3+ cells in human PBL are heterogeneous in function and include not only suppressive T cells but also nonsuppressive ones that abundantly secrete proinflammatory cytokines such as IL-17. Further, Treg cells functionally and phenotypically differentiate within the FoxP3+ population. This functional heterogeneity and differentiation dynamics can be clearly shown by separating FoxP3+ cells into three subsets based on the expression of FoxP3 and CD45RA (or CD45RO), which

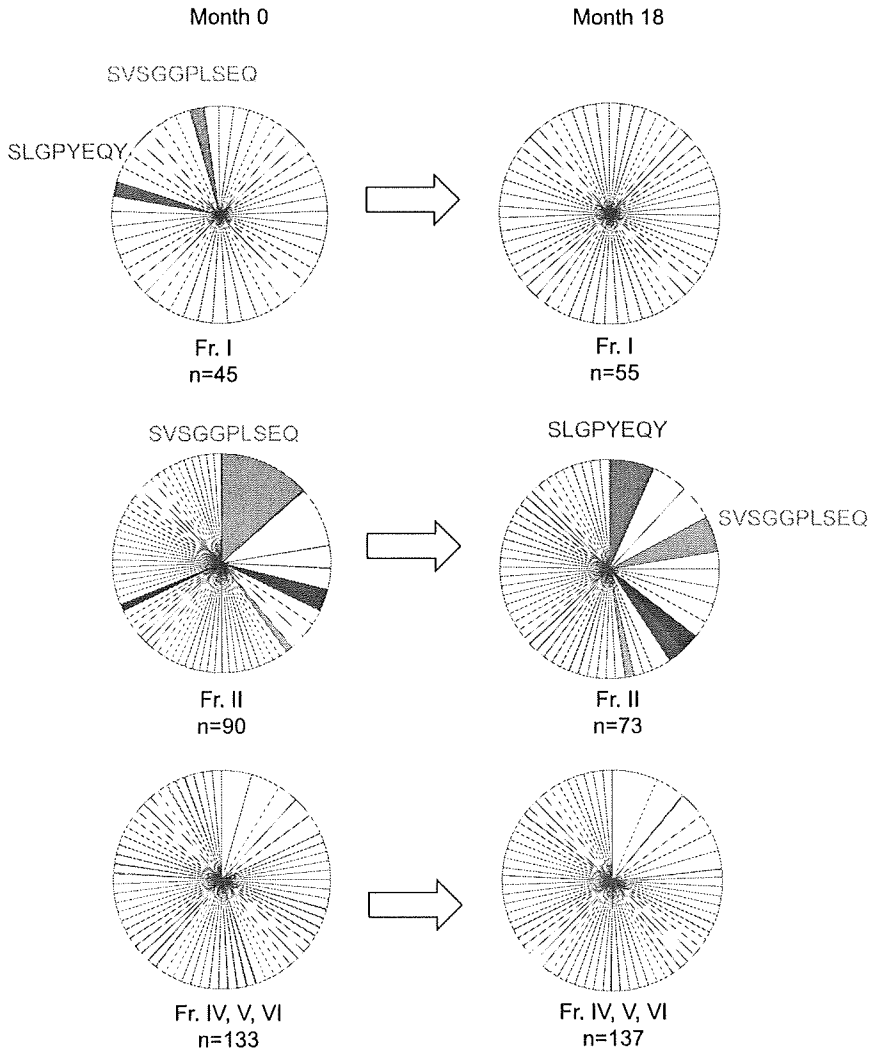

Figure 5. Longitudinal TCR Repertoire Analysis in FoxP3+ Cell Subpopulations

TCRBV5+CD4+ T cells belonging to indicated Treg or non-Treg cell fractions were FACS sorted as a single cell at indicated time points into wells of PCR plates. By RT-PCR and TCR sequencing, the frequencies of individual sequences were assessed. Empty slices correspond to sequences that were found only once in only one subset. Persistent clones are color highlighted. Slice size is proportional to the number of occurrences of the corresponding TCR sequences. The total number of sequences successfully analyzed in each subset is indicated.

controls signaling thresholds in lymphocytes, hence their state of differentiation and activation (Hermiston et al., 2003). The three subpopulations are CD45RA$^-$FoxP3^{hi}CD4$^+$ activated Treg cells and CD45RA$^+$FoxP3^{lo}CD4$^+$ resting Treg cells, both of which are potently suppressive in vitro, and cytokine-secreting nonsuppressive CD45RA$^-$FoxP3^{lo}CD4$^+$ non-Treg cells.

The distinction of FoxP3$^+$ subpopulations revealed the differentiation pathways of Treg cell subpopulations. First, most of FoxP3^{hi} aTreg cells originate from rTreg cells as shown in vitro and in vivo, although some FoxP3^{hi} Treg cells may arise from FoxP3$^-$CD4$^+$ non-Treg cells (Vukmanovic-Stejic et al., 2006). Second, a large proportion of FoxP3^{hi} aTreg cells is highly proliferative in vivo and appears to be recently activated, although most rTreg cells are in a resting state. Once rTreg cells are stimulated, they upregulate FoxP3 expression, differentiate to aTreg cells, and proliferate. In addition to these results obtained by direct ex vivo analysis of the subpopulations and by their transfer to NOG mice, our longitudinal study of the repertoire of a particular TCR Vβ subfamily in a single individual provides further evidence that the conversion of rTreg to aTreg cells physiologically occurs in vivo. In our current analysis, dominant clones found in the rTreg cell population were found 18 months later in the aTreg, but not rTreg, cell population. This indicates that the clones have preferentially expanded after differentiating to aTreg cells, as suggested by the high rate of Ki-67$^+$ cells in the aTreg cell population. The presence of such dominant T cell clones over a long period of time is a key feature of the aTreg cell population (C.P. and G.G., unpublished data). This also indicates that the TCR repertoire of Treg cells adaptively changes with clonal expansion especially in aTreg cells. Considering that aTreg cells rapidly die in vitro and that the immune system is constantly challenged by exogenous and endogenous antigens, it is highly likely that the maintenance of the pool of aTreg cells is the consequence of a tight balance between the constant development of aTreg cells from activated and proliferating rTreg cells and their death after exerting suppression. Further, aTreg cells control rTreg cell expansion in a feedback manner, contributing to the maintenance of the balance. FoxP3^{hi} aTreg cells thus appear to be terminally differentiated Treg cells; yet it remains to be determined whether the aTreg cell population contains a memory type long-living Treg cells. Given that aTreg cells die rapidly and that rTreg cells are highly proliferative upon stimulation, attempts to expand Treg cells ex vivo for cell therapy should be focused on rTreg cells as proposed by others (Hoffmann et al., 2006). It needs to be determined whether rTreg cells are constantly produced by the thymus, or whether they have a high renewal capacity in the periphery, or both.

Our study has clearly shown that human FoxP3$^+$CD4$^+$ T cells contain cytokine-secreting nonsuppressive effector T cells that display low expression of FoxP3. These nonsuppressive FoxP3^{lo}CD45RA$^-$CD4$^+$ T cells (Fr. III) may correspond to recently described activation-induced FoxP3-expressing cells that transiently express FoxP3 in vitro (Allan et al., 2007; Gavin et al., 2006; Tran et al., 2007; Wang et al., 2007). Supporting this notion, although the 5′ flanking region of the *FOXP3* gene in FoxP3^{lo}CD45RA$^-$CD4$^+$ T cells is highly demethylated, the STAT5-responsive region is poorly demethylated, suggesting that they may be unstable in maintaining FoxP3 expression through

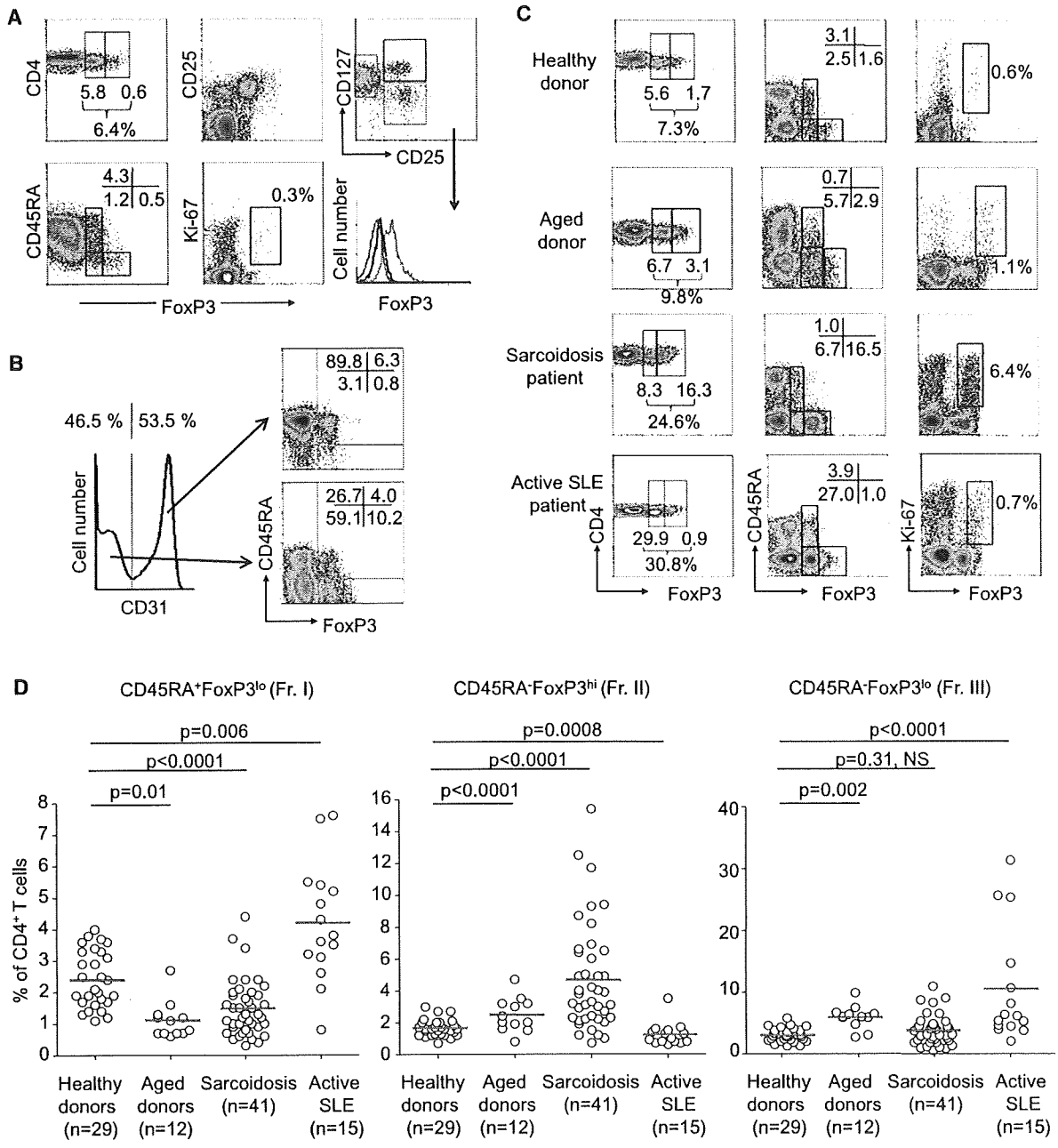

Figure 6. Variations in FoxP3+ Cell Subpopulations under Physiological and Disease Conditions

(A) Flow cytometry of PBMCs gated on $CD4^+$ T cells isolated from cord blood. A representative of four samples.

(B) Expression of CD45RA and FoxP3 by gated $CD31^+$ or $CD31^-$ $CD4^+$ T cells. Numbers indicate percentage in each quadrant. A representative of four independent experiments.

(C) Flow cytometry of PBMCs gated on $CD4^+$ T cells isolated from a 29-year-old healthy adult, an 88-year-old donor, and two patients with active sarcoidosis or active SLE. Percentage of each quadrant in each staining combination is shown.

(D) Percentages of each FoxP3+ subset among $CD4^+$ T cells in indicated numbers of patients with active sarcoidosis, active SLE, aged donors (between 79 and 90 years old), and healthy donors (between 18 and 40 years old). Red horizontal bars represent mean percentage. Statistical comparisons were performed by nonparametric Mann-Whitney U test. NS, not significant.

STAT5 signaling. The notion is also supported by recent reports showing that activation-induced $FoxP3^+CD4^+$ T cells have *FOXP3* DNA significantly less demethylated than bona fide Treg cells (Baron et al., 2007; Janson et al., 2008). In addition, although CD127 is a convenient marker for isolating $FoxP3^+$ cells as $CD25^{hi}CD127^{lo}CD4^+$ T cells (Liu et al., 2006; Seddiki et al., 2006), it is of note that they also include $FoxP3^+$ non-Treg cells. We therefore propose that the combination of CD25 and CD45RA is so far the best markers for purifying human $FoxP3^+$ Treg cells as rTreg and aTreg cells.